 CMC, vol.19, no.2, pp.155-198, 2010

RMVT- and PVD-Based Finite Layer Methods for the Quasi-3D Free Vibration Analysis of Multilayered Composite and FGM Plates

Chih-Ping Wu[1,2] **and Hao-Yuan Li**[2]

Abstract: The Reissner mixed variational theorem (RMVT)- and principle of virtual displacements (PVD)-based finite layer methods (FLMs) are developed for the quasi-three-dimensional (3D) free vibration analysis of simply-supported, multilayered composite and functionally graded material (FGM) plates. The material properties of the FGM layers are assumed to obey either an exponent-law exponentially varied with the thickness coordinate or the power-law distributions of the volume fractions of the constituents. In these formulations, the plate is divided into a number of finite layers, where the trigonometric functions and Lagrange polynomials are used to interpolate the in- and out-of-plane variations of the field variables of each individual layer, respectively. Because an *h*- rather than *p*-refinement process is adopted to yield the convergent solutions in this analysis, a layerwise linear or parabolic function distribution through the thickness coordinate is assumed for the related field variables. The unified formulations of these two kinds of FLMs with freely-chosen orders are presented, which are used for expansion of in- and out-of-plane field variables through the thickness coordinate. The natural frequencies and their corresponding modal field variable distributions through the thickness coordinate of the multilayered composite and FGM plates are studied using the various RMVT- and PVD-based FLMs developed in this paper, and the accuracy and convergence rate of these are assessed by comparing their solutions with the exact 3D solutions available in the literature.

Keywords: Reissner, Mixed theories, Principle of virtual displacements, Finite layer methods, Functionally graded materials, Plates.

[1] Corresponding author. *E-mail*: cpwu@mail.ncku.edu.tw; *Fax*: +886-6-2370804
[2] Department of Civil Engineering, National Cheng Kung University, Taiwan, ROC

1 Introduction

In recent decades, functional graded materials (FGMs) have been developed to replace fiber reinforced composite materials as a new generation of engineering materials, and have been widely utilized in various advanced industrial structures, with beam-, plate- and shell-like forms. Unlike the multilayered composite structures, in which the material properties are layerwise constant-varied through the thickness coordinate, the material properties of multilayered FGM structures vary smoothly and continuously throughout. Because of this superior feature of the multilayered FGM structures, some drawbacks of conventional multilayered composite structures resulting from the abrupt changes of material properties at the interfaces between adjacent layers have been overcome, such as residual stress concentration, de-lamination and matrix cracking. The development of theoretical methodologies and numerical modeling for the analysis of this new class of FGM plates/shells has thus attracted considerable attention, and some comprehensive literature surveys for the computational models of multilayered composite and FGM plates/shells have been undertaken (Noor and Burton, 1990a, b, 1992; Soldatos, 1994; Tang et al., 1996; Saravanos and Heyliger, 1999; Carrera, 2000a, b, 2003a, 2004; Wu et al., 2008). Among the various computational models, we will focus on the discrete layer ones for the static and free vibration analyses of multilayered composite and FGM plates in this paper.

Sciuva (1986) developed a discrete layer first-order shear deformation theory (FSDT) for the bending, vibration and buckling of simply supported thick multilayered orthotropic plates. Based on a discrete layer third-order shear deformation theory (TSDT), Cho et al. (1991) studied the free vibration of laminated rectangular plates, in which the natural frequencies and their corresponding modal stress and displacement distributions through the thickness coordinate were determined. A generalized discrete layer TSDT was developed by Kant and Swaminathan (2001) for the free vibration analysis of laminated composite and sandwich plates, in which the warping of the transverse cross-section was modeled more realistically than in the other discrete layer theories in the literature. Wu and Kuo (1992, 1993) and Wu and Chen (1994) developed a local TSDT and its related mixed finite element method (FEM) for the static and free vibration analyses of multilayered composite plates, in which the displacement and transverse stress continuity conditions at the interfaces between adjacent layers were imposed as the constraints and introduced into the potential energy functional by the Lagange multiplier method.

Based on a discrete layer theory combined with the Ritz method, Ramirez, Heyliger and Pan (2006a, b) investigated the static behaviors of functionally graded (FG) elastic plates and the free vibration responses of FG magneto-electro-elastic plates. Hussein and Heyliger (1996) presented a semi-analytical discrete layer theory,

where the unknown field variables were formed by combining the finite element approximations through the thickness coordinate with Fourier and/or power series in the axial and circumferential coordinates, for the analysis of axisymmetric laminated cylindrical shells with distributed piezoelectric layers. Saravanos et al. (1997) developed a finite element formulation for the quasi-static and dynamic analyses of smart composite plates using the layerwise representations of displacements and electric potential. Based on the principle of virtual displacements (PVD), Carrera (2003b) and Demasi (2008) developed the Carrera and Generalized Unified Formulations (CUF and GUF), respectively, for the analysis of multilayered composite plates. In the CUF, the order of each displacement variable expanded in the thickness coordinate remains the same, and can be freely chosen. Morever, the stiffness (or compliance) matrices of all possible theories are generated from the expansion of 3 by 3 matrices (fundamental nuclei). In the case of GUF, the order of each displacement variable expanded in the thickness coordinate can be independently chosen with respect to the others. The stiffness (or compliance) matrices of all possible theories are generated from the expansion of 1 by 1 matrices.

These multilayered composite and FGM plate theories and their related numerical models are all based on the PVD, where the generalized displacement components are regarded as the primary variables, and the in-plane stress components can be calculated from the determined primary variables using Hooke's law. While these theories might give an accurate prediction on the displacement and in-plane stress components of the deformed multilayered composite and FGM plates/shells, they might fail to yield the same accuracy for the transverse shear and normal stresses. A subsequent correction process for the calculation of transverse shear and normal stresses is thus usually needed to improve the accuracy for those stresses, where they are calculated using the integrations derived from the stress equilibrium equations.

Another variational theorem, namely the Reissner Mixed Variational Theorem (RMVT), was proposed by Reissner (1984, 1986) for the analysis of laminated composite plates, where the displacement and transverse stress components are regarded as the primary variables and the in-plane stress components can be calculated by the primary variables that are determined. The related developments, ideas, and evaluations based on the RMVT with regard to the modeling of multilayered plates were described by Carrera (2001). Based on the RMVT, Murakami (1986) and Toledano and Murakami (1987) proposed the mixed laminated plate theories with global first-order and higher-order zig-zag displacement models, respectively, to improve the in-plane responses of the laminated composite plates. Based on Toledano and Murakami's mixed plate model, Carrera (1999) studied the effect of transverse normal stress on vibration of multilayered composite plates and shells. The CUF and

GUF mentioned above can also be extensively applied to the theories based on the RMVT, and a variety of the so-called PVD- and RMVT-based equivalent single layer theories (ESLTs) can be included as special cases of the CUF and GUF. Carrera et al. (2008) combined the CUF with a variable kinematic (VK) model to investigate the static behavior of FGM plates, in which both the closed-form and finite element solutions were presented. The CUF has also been extensively used to study the static behaviors of functionally graded (FG) elastic and piezoelectric plates by Brischetto et al. (2008) and Brischetto and Carrera (2009). Based on the RMVT instead of PVD, Brischetto and Carrera (2008) developed a GUF for the bending analysis of FGM plates, in which various RMVT-based ESLTs were included as special cases. Zenkour (2006) developed a generalized shear deformation theory for the bending analysis of FGM plates. On the basis of RMVT, Kant et al. (2007) presented a general partial discritization methodology for interlaminar stress computation in composite laminates. Desai et al. (2003) developed a discrete layer finite element model on the basis of the RMVT for the three-dimensional (3D) dynamic analysis of laminated composite plates. In conjunction with the Reddy third-order displacement model and the RMVT, Wu and Li (2010a) presented an RMVT-based TSDT for the analysis of multilayered composite and FGM plates, which was also studied by Wu and Li (2010b) using the RMVT- and PVD-based finite layer methods (FLMs), and Wu et al. (2010) using the meshless collocation and element-free Galerkin methods. A series of five articles with regard to the development of a RMVT-based generalized unified formulation and its applications to the multilayered composite plates were presented by Demasi (2009a–e), in which a variety of RMVT-based first-order and higher-order shear deformation, zig-zag, and layerwise theories were included.

Some 3D solutions of multilayered composite and FGM plates and shells are available in the literature. Pagano (1969, 1970) presented a classical method for the 3D analysis of multilayered composite elastic strips under cylindrical bending and with sandwich plates under the sinusoidally distributed load, and this classical method was also extended to the 3D bending, vibration and buckling problems of rectangular laminated composite plates by Srinivas and Rao (1970). Based on the 3D elasticity and thermoelasticity, Noor (1990c), Savoia and Reddy (1995) and Kardomateas (2009) presented 3D solutions for the static analysis of rectangular multilayered composite and sandwich plates under mechanical and thermomechanical loads, which was also studied by zenkour (2007) and Demasi (2008a, 2008b) using the state space, as well as 2D, quasi 3D and 3D elasticity approaches, in which Demasi's work extended the GUF to the case of orthotropic materials, and the corresponding ∞^3 theories were presented. Carrera et al. (2010) developed some 3D and 2D closed form plate models for the static analysis of simply supported

square isotropic plates, in which attention is mainly paid on localized loading conditions. Vel and Batra (2001, 2002, 2003, 2004) presented the 3D solutions for the thermoelastic deformations, and free and forced vibrations of FG elastic plates, as well as the cylindrical bending of laminated plates with embedded piezoelectric shear actuators using the power series method, in which the effective material property distributions through the thickness coordinate were estimated using either the Mori-Tanaka (Mori and Tanaka, 1973) or self-consistent (Hill, 1965) schemes. Kashtalyan (2004) presented the 3D elasticity solution for bending of FG isotropic plates, in which the Young's modulus of the plate was assumed to vary exponentially through the thickness coordinate, and the Poisson's ratio to be constant. Lü et al. (2007, 2008) developed a 3D semi-analytical method for the cylindrical bending vibration of angle-ply laminated composite plates and the static behavior of laminated composite plates. Li et al. (2008) presented the 3D free vibration analysis of FGM sandwich plates, in which the displacement components were expanded by a series of Chebyshev polynomials multiplied by appropriate functions satisfying the essential boundary conditions, and a 3D Ritz method was used to determine the natural frequencies of the sandwich plates. Pan (2003) studied a three-dimensional (3D) exact analysis of FG anisotropic elastic plates using the state space formulation, which was also extended to the static and dynamic analyses of multilayered and FGM plates by Heyliger (1997), Pan and Heyliger (2002), and Pan and Han (2005). A series of 3D dynamic analysis of multilayered composite and FGM plates and shells was also presented using the multiple scale (Wu et al., 1996, 1998; Wu and Wu, 2000; Wu and Tsai, 2009, 2010) and modified Pagano methods (Wu and Lü, 2009). Finally, a review of the 3D analytical approaches of multilayered and FG piezoelectric plates and shells was undertaken by Wu, Chiu and Wang (2008). These early 3D solutions may provide a reference for our kinematic and kinetic assumptions a priori when we are deriving a 2D theory of FGM plates, and may act as a standard for us to assess the various 2D theories of multilayered FGM plates in the literature.

A finite layer method (FLM), which is extended from the finite strip method (Cheung, 1976) was used to study the 3D static problems of piezoelectric composite laminates by Cheung and Jiang (2001). In the FLM, the simply-supported laminate is divided into a number of finite layers, and the trigonometric functions and Lagrange polynomials are used to interpolate the in- and out-of-plane variations of the field variables, respectively, for each individual layer. It has been demonstrated that a semi-analytical FLM is more effective in reducing computational effort and core requirements for simply supported laminates. This FLM was also extended to the 3D static, vibration and stability as well as thermal buckling analyses of piezoelectric composite plates by Akhras and Li (2007, 2008). Again, the FLMs mentioned

above were also based on the PVD rather than the RMVT. Thus, Wu and Li (2010b) developed the RMVT- and PVD-based FLMs to investigate the quasi-3D static behavior of multilayered and FGM plates, in which the unified formulations of these two FLMs with freely-chosen orders used for the expansions of the in- and out-of-plane field variables through the thickness coordinate were presented, and an h-refinement process was used to yield the convergent solutions.

In this paper, the RMVT- and PVD-based FLMs mentioned above are extended to the quasi-3D free vibration analysis of multilayered composite and FGM plates. The system motion equations are derived using the Hamilton principle. The solutions of the natural frequencies and their corresponding modal field variable distributions through the thickness coordinate are determined and compared with the 3D solutions available in the literature to assess their convergence rate and accuracy. The numerical instability (Demasi, 2009e), resulting from the relative orders used for the expansion of the stresses and displacements in RMVT- and PVD-based FLMs, is also examined. Finally, a parametric study of the effects of the material-property gradient index and the span-thickness ratio on the natural frequencies and their modal field variable distributions through the thickness coordinate of the FGM plates is undertaken.

2 RMVT-based finite layer methods

2.1 The kinematic and kinetic assumptions

We consider a simply supported, multilayered composite and FGM plate, as shown in Fig. 1a. A Cartesian global coordinate system (x, y and ζ coordinates) is located on the middle plane of the plate; and a set of Cartesian local thickness coordinates, $z_m\,(m = 1,\ 2,\ 3, \cdots,\ N)$, is located at the mid-plane of each individual layer, as shown in Fig. 1b, where N is the total number of the layers constituting the plate, and is taken to be three as a special case. The thicknesses of each individual layer and the plate are $h_m\ (m = 1,\ 2, \cdots,\ N)$ and h, respectively, and $h = \sum_{m=1}^{N} h_m$. L_x and L_y denote the in-plane dimensions in the x and y directions, respectively. The relationship between the global and local thickness coordinates in the m^{th}-layer is $\zeta = \bar{z}_m + z_m$, in which $\bar{z}_m = (\zeta_m + \zeta_{m-1})/2$, and ζ_m and ζ_{m-1} are the global thickness coordinates measured from the mid-plane of the plate to the top and bottom surfaces of the m^{th}-layer, respectively.

A discrete layer displacement model with either linear or quadratic function distributions through the thickness coordinate for the displacements is adopted as the kinematic field of the m^{th}-layer of the plate in the present formulation, of which the

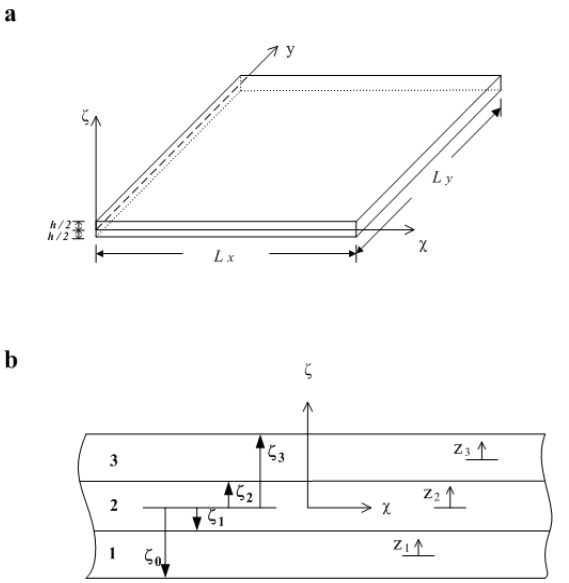

Figure 1: The configuration and coordinates of a multilayered FGM plate.

domain is in $0 \leq x \leq L_x$, $0 \leq y \leq L_y$ and $(-h_m/2) \leq z_m \leq (h_m/2)$, and is given by

$$u_x^{(m)}(x, y, z_m, t) = \sum_{i=1}^{N_u+1} \left[\psi_u^{(m)}(z_m)\right]_i \left[u^{(m)}(x, y, t)\right]_i, \tag{1}$$

$$u_y^{(m)}(x, y, z_m, t) = \sum_{i=1}^{N_u+1} \left[\psi_u^{(m)}(z_m)\right]_i \left[v^{(m)}(x, y, t)\right]_i, \tag{2}$$

$$u_\zeta^{(m)}(x, y, z_m, t) = \sum_{j=1}^{N_w+1} \left[\psi_w^{(m)}(z_m)\right]_j \left[w^{(m)}(x, y, t)\right]_j, \tag{3}$$

where t is the time variable; $(u_x^{(m)},\ u_y^{(m)},\ u_\zeta^{(m)})$ denote the displacement components of the m^{th}-layer of the plate in the x, y and ζ directions, respectively; $\left(u^{(m)}\right)_i$, $\left(v^{(m)}\right)_i$, $\left(w^{(m)}\right)_j$ with $(i = 1, 2, \cdots, N_u + 1)$ and $(j = 1, 2, \cdots, N_w + 1)$ are the displacement components at the nodal planes of the m^{th}-layer of the plate; and $\left(\psi_u^{(m)}\right)_i$ $(i = 1, \cdots, N_u + 1)$ and $\left(\psi_w^{(m)}\right)_j$ $(j = 1, 2, \cdots, N_w + 1)$ are the corresponding shape functions, in which N_u and N_w denote the related orders used for the expansion of the in-plane and out-of-plane displacements, respectively. For

the quadratic and linear layers, the shape functions in the thickness coordinate are given as follows:

For a quadratic layer with three nodal planes (i.e., $N_k = 2,$ and $k = u$ or w), they are

$$\left[\psi_k^{(m)}(z_m)\right]_1 = \left(2/h_m^2\right) z_m (z_m - h_m/2),$$

$$\left[\psi_k^{(m)}(z_m)\right]_2 = \left(2/h_m^2\right) z_m (z_m + h_m/2),$$

$$\left[\psi_k^{(m)}(z_m)\right]_3 = -\left(4/h_m^2\right) (z_m + h_m/2) (z_m - h_m/2);$$

and for a linear layer with two nodal planes (i.e., $N_k = 1,$ and $k = u$ or w), they are

$$\left[\psi_k^{(m)}(z_m)\right]_1 = (-1/h_m) (z_m - h_m/2),$$

$$\left[\psi_k^{(m)}(z_m)\right]_2 = (1/h_m) (z_m + h_m/2).$$

The transverse shear and normal stresses are regarded as the primary variables in the present RMVT-based rather than PVD-based FLMs, and are assumed as follows:

$$\tau_{x\zeta}^{(m)}(x, y, z_m, t) = \sum_{i=1}^{N_\tau+1} \left[\psi_\tau^{(m)}(z_m)\right]_i \left[\tau_{13}^{(m)}(x, y, t)\right]_i, \tag{4}$$

$$\tau_{y\zeta}^{(m)}(x, y, z_m, t) = \sum_{i=1}^{N_\tau+1} \left[\psi_\tau^{(m)}(z_m)\right]_i \left[\tau_{23}^{(m)}(x, y, t)\right]_i, \tag{5}$$

$$\sigma_{\zeta}^{(m)}(x, y, z_m, t) = \sum_{i=1}^{N_\sigma+1} \left[\psi_\sigma^{(m)}(z_m)\right]_i \left[\sigma_3^{(m)}(x, y, t)\right]_i, \tag{6}$$

where $\left(\tau_{13}^{(m)}\right)_i$, $\left(\tau_{23}^{(m)}\right)_i$, $\left(\sigma_3^{(m)}\right)_j$ with $(i = 1, 2, \cdots, N_\tau + 1)$ and $(j = 1, 2, \cdots, N_\sigma + 1)$ are the transverse stress components at the nodal planes of the m^{th}-layer of the plate; and $(\psi_\tau^{(m)})_i$ $(i = 1, 2, \cdots, N_\tau + 1)$ and $\left(\psi_\sigma^{(m)}\right)_i$ $(i = 1, 2, \cdots, N_\sigma + 1)$ are the corresponding shape functions, in which N_τ and N_σ denote the related orders used for the expansion of the transverse shear and normal stresses, respectively.

According to Demasi (2009e), it is concluded that the relative orders used for the expansions of the in-plane and out-of-plane displacements, as well as the transverse shear and normal stresses, should be the crucial assumptions for the RMVT-based

plate/shell theories, because these assumptions can be the source of numerical instabilities. The orders of various displacements and transverse stresses are thus taken to be variable, and can be freely-chosen, as in the present formulations (i.e., either $N_i = 1$ or $N_i = 2$ for an h-refinement process, in which $i = u,\ w,\ \tau$ and σ). The relevant numerical instability for various RMVT-based FLMs will be investigated later in this paper.

The linear constitutive equations for the m^{th}-layer, which are valid for the orthotropic materials, are given by

$$\begin{Bmatrix} \sigma_x^{(m)} \\ \sigma_y^{(m)} \\ \sigma_\zeta^{(m)} \\ \tau_{y\zeta}^{(m)} \\ \tau_{x\zeta}^{(m)} \\ \tau_{xy}^{(m)} \end{Bmatrix} = \begin{bmatrix} c_{11}^{(m)} & c_{12}^{(m)} & c_{13}^{(m)} & 0 & 0 & 0 \\ c_{12}^{(m)} & c_{22}^{(m)} & c_{23}^{(m)} & 0 & 0 & 0 \\ c_{13}^{(m)} & c_{23}^{(m)} & c_{33}^{(m)} & 0 & 0 & 0 \\ 0 & 0 & 0 & c_{44}^{(m)} & 0 & 0 \\ 0 & 0 & 0 & 0 & c_{55}^{(m)} & 0 \\ 0 & 0 & 0 & 0 & 0 & c_{66}^{(m)} \end{bmatrix} \begin{Bmatrix} \varepsilon_x^{(m)} \\ \varepsilon_y^{(m)} \\ \varepsilon_\zeta^{(m)} \\ \gamma_{y\zeta}^{(m)} \\ \gamma_{x\zeta}^{(m)} \\ \gamma_{xy}^{(m)} \end{Bmatrix}, \tag{7}$$

where $(\sigma_x^{(m)},\ \sigma_y^{(m)},\ \cdots,\ \tau_{xy}^{(m)})$ are the stress components; $(\varepsilon_x^{(m)},\ \varepsilon_y^{(m)},\ \cdots,\ \gamma_{xy}^{(m)})$ are the strain components; and $c_{ij}^{(m)}$ are the elastic coefficients, which are constants through the thickness coordinate in the homogeneous elastic layers, and variable through the thickness coordinate in the FG elastic layers (i.e., $c_{ij}^{(m)}(\zeta)$).

The strain-displacement relations for each individual layer, based on the assumed displacement model in Eqs. (1)–(3), are given by

$$\begin{aligned} \varepsilon_x^{(m)} &= u_x^{(m)},_x \\ &= \sum_{i=1}^{N_u+1} \psi_u^{(m)}\, u_i^{(m)},_x \end{aligned}, \tag{8}$$

$$\begin{aligned} \varepsilon_y^{(m)} &= u_y^{(m)},_y \\ &= \sum_{i=1}^{N_u+1} \psi_u^{(m)}\, v_i^{(m)},_y \end{aligned}, \tag{9}$$

$$\begin{aligned} \varepsilon_\zeta^{(m)} &= u_\zeta^{(m)},_\zeta \\ &= \sum_{i=1}^{N_w+1} D\psi_w^{(m)}\, w_i^{(m)} \end{aligned}, \tag{10}$$

$$\begin{aligned} \gamma_{y\zeta}^{(m)} &= u_x^{(m)},_\zeta + u_\zeta^{(m)},_x \\ &= \sum_{i=1}^{N_u+1} D\psi_u^{(m)}\, u_i^{(m)} + \sum_{i=1}^{N_w+1} \psi_w^{(m)}\, w_i^{(m)},_x \end{aligned}, \tag{11}$$

$$\gamma_{x\zeta}^{(m)} = u_y^{(m)},_{\zeta} + u_{\zeta}^{(m)},_y = \sum_{i=1}^{N_u+1} D\psi_u^{(m)}\, v_i^{(m)} + \sum_{i=1}^{N_w+1} \psi_w^{(m)}\, w_i^{(m)},_y \quad , \tag{12}$$

$$\gamma_{xy}^{(m)} = u_x^{(m)},_y + u_y^{(m)},_x = \sum_{i=1}^{N_u+1} \psi_u^{(m)}\, u_i^{(m)},_y + \sum_{i=1}^{N_u+1} \psi_u^{(m)}\, v_i^{(m)},_x \quad , \tag{13}$$

where the commas denote partial differentiation with respect to the suffix variables; and $D\psi_j^{(m)} = \frac{d\psi_j^{(m)}}{dz_m}$ $(j = u,\ w,\ \tau$ and $\sigma)$.

2.2 The RMVT-based Hamilton principle

The RMVT-based Hamilton principle is used to derive the motion equations of the plate for the RMVT-based FLMs, and its corresponding energy functional for the plate is written in the form of

$$I_R = \int_{t_1}^{t_2} (T - V_R)\, dt, \tag{14}$$

where T and V_R denote the kinetic and RMVT-based potential energy of the plate, respectively, and given as

$$T = \sum_{m=1}^{N} \int_{-h_m/2}^{h_m/2} \iint_{\Omega} \frac{\rho^{(m)}}{2} \left[\left(u_x^{(m)},_t\right)^2 + \left(u_y^{(m)},_t\right)^2 + \left(u_{\zeta}^{(m)},_t\right)^2 \right] dx\, dy\, dz_m,$$

$$\begin{aligned} V_R = & \sum_{m=1}^{N} \int_{-h_m/2}^{h_m/2} \iint_{\Omega} \left[\sigma_x^{(m)} \varepsilon_x^{(m)} + \sigma_y^{(m)} \varepsilon_y^{(m)} + \sigma_{\zeta}^{(m)} \varepsilon_{\zeta}^{(m)} + \tau_{x\zeta}^{(m)} \gamma_{x\zeta}^{(m)} + \tau_{y\zeta}^{(m)} \gamma_{y\zeta}^{(m)} \right. \\ & \left. + \tau_{xy}^{(m)} \gamma_{xy}^{(m)} - B\left(\sigma_{ij}^{(m)}\right) \right] dx\, dy\, dz_m \\ & - \sum_{m=1}^{N} \int_{-h_m/2}^{h_m/2} \int_{\Gamma_\sigma} \left(\bar{t}_x^{(m)} u_x^{(m)} + \bar{t}_y^{(m)} u_y^{(m)} + \bar{t}_{\zeta}^{(m)} u_{\zeta}^{(m)} \right) d\Gamma\, dz_m \\ & - \sum_{m=1}^{N} \int_{-h_m/2}^{h_m/2} \int_{\Gamma_u} \left[(u_x^{(m)} - \bar{u}_x^{(m)})\, t_x^{(m)} + (u_y^{(m)} - \bar{u}_y^{(m)})\, t_y^{(m)} \right. \\ & \left. + (u_{\zeta}^{(m)} - \bar{u}_{\zeta}^{(m)})\, t_{\zeta}^{(m)} \right] d\Gamma\, dz_m, \end{aligned}$$

in which $\rho^{(m)}$ is the mass density of the mth-layer; Ω denotes the plate domain on the $x-y$ plane; Γ_σ and Γ_u denote the portions of the edge boundary, where the surface traction and displacement components (i.e., $\bar{t}_i^{(m)}$, $\bar{u}_i^{(m)}$ in which i=x, y and z_m) are prescribed, respectively; and $B(\sigma_{ij}^{(m)})$ is the complementary density function.

In the present formulation, we take the displacement and the transverse stress components to be the primary variables subject to variation. By using the kinematic and kinetic assumptions given in Eqs. (1)–(3) and (4)–(6), we may express the first-order variation of the energy functional I_R as follows:

$$\delta I_R = \int_{t_1}^{t_2} (\delta T - \delta V_R)\, dt, \tag{15}$$

where

$$\delta T = \iint_\Omega \sum_{m=1}^{N} \int_{-h_m/2}^{h_m/2} \rho^{(m)} \left[\left(\delta \mathbf{u}_p^{(m)},_t \right)^T \mathbf{u}_p^{(m)},_t + \left(\delta u_\zeta^{(m)},_t \right) u_\zeta^{(m)},_t \right] dx\, dy\, dz_m,$$

$$\begin{aligned}
\delta V_R = \iint_\Omega \sum_{m=1}^{N} \int_{-h_m/2}^{h_m/2} \Bigg\{ & \left(\delta \varepsilon_p^{(m)} \right)^T \sigma_p^{(m)} + \left(\delta \varepsilon_s^{(m)} \right)^T \sigma_s^{(m)} + \delta \varepsilon_\zeta\, \sigma_\zeta^{(m)} \\
& + \left(\delta \sigma_s^{(m)} \right)^T \left(\varepsilon_s^{(m)} - \mathbf{S}^{(m)} \sigma_s^{(m)} \right) \\
& + \delta \sigma_\zeta^{(m)} \left[\varepsilon_\zeta^{(m)} - \left(c_{33}^{(m)} \right)^{-1} \sigma_\zeta^{(m)} - \left(\mathbf{Q}_\zeta^{(m)} \right)^{\mathrm{T}} \varepsilon_p^{(m)} \right] \Bigg\} dx\, dy\, dz_m \\
& - \sum_{m=1}^{N} \int_{-h_m/2}^{h_m/2} \int_{\Gamma_\sigma} \left(\bar{t}_x^{(m)} \delta u_x^{(m)} + \bar{t}_y^{(m)} \delta u_y^{(m)} + \bar{t}_\zeta^{(m)} \delta u_\zeta^{(m)} \right) d\Gamma\, dz_m \\
& - \sum_{m=1}^{N} \int_{-h_m/2}^{h_m/2} \int_{\Gamma_u} \Big[(u_x^{(m)} - \bar{u}_x^{(m)})\, \delta t_x^{(m)} + (u_y^{(m)} - \bar{u}_y^{(m)})\, \delta t_y^{(m)} \\
& + (u_\zeta^{(m)} - \bar{u}_\zeta^{(m)})\, \delta t_\zeta^{(m)} \Big]\, d\Gamma\, dz_m;
\end{aligned}$$

$$\varepsilon_p^{(m)} = \begin{bmatrix} \varepsilon_x^{(m)} & \varepsilon_y^{(m)} & \gamma_{xy}^{(m)} \end{bmatrix}^T = \mathbf{B}_1^{(m)} \mathbf{u}^{(m)},$$

$$\varepsilon_s^{(m)} = \begin{bmatrix} \gamma_{x\zeta}^{(m)} & \gamma_{y\zeta}^{(m)} \end{bmatrix}^T = \mathbf{B}_3^{(m)} \mathbf{u}^{(m)} + \mathbf{B}_4^{(m)} \mathbf{w}^{(m)},$$

$$\varepsilon_\zeta^{(m)} = \mathbf{B}_6^{(m)} \mathbf{w}^{(m)},$$

$$\sigma_p^{(m)} = \begin{bmatrix} \sigma_x^{(m)} & \sigma_y^{(m)} & \tau_{xy}^{(m)} \end{bmatrix}^T = \mathbf{Q}_p^{(m)} \mathbf{B}_1^{(m)} \mathbf{u}^{(m)} + \mathbf{Q}_\zeta^{(m)} \mathbf{B}_2^{(m)} \sigma^{(m)},$$

$$\sigma_s^{(m)} = \begin{bmatrix} \tau_{x\zeta}^{(m)} & \tau_{y\zeta}^{(m)} \end{bmatrix}^T = \mathbf{B}_5^{(m)} \tau^{(m)}, \quad \sigma_\zeta^{(m)} = \mathbf{B}_2^{(m)} \sigma^{(m)},$$

$$\mathbf{u}_p^{(m)} = \begin{bmatrix} u_x^{(m)} & u_y^{(m)} \end{bmatrix}^T = \mathbf{B}_7^{(m)} \mathbf{u}^{(m)}, \quad u_\zeta^{(m)} = \mathbf{B}_8^{(m)} \mathbf{w}^{(m)},$$

$$\mathbf{u}^{(m)} = \begin{bmatrix} u_i^{(m)} \\ v_i^{(m)} \end{bmatrix}_{i=1,2,\cdots,N_u+1}, \quad \mathbf{w}^{(m)} = \left[w_i^{(m)} \right]_{i=1,2,\cdots,N_w+1},$$

$$\tau^{(m)} = \begin{bmatrix} \left(\tau_{13}^{(m)}\right)_i \\ \left(\tau_{23}^{(m)}\right)_i \end{bmatrix}_{i=1,2,\cdots,N_\tau+1}, \quad \sigma^{(m)} = \left[\left(\sigma_3^{(m)}\right)_i \right]_{i=1,2,\cdots,N_\sigma+1},$$

$$\mathbf{S}^{(m)} = \begin{bmatrix} \left(1/c_{55}^{(m)}\right) & 0 \\ 0 & \left(1/c_{44}^{(m)}\right) \end{bmatrix}, \quad \mathbf{Q}_p^{(m)} = \begin{bmatrix} Q_{11}^{(m)} & Q_{12}^{(m)} & 0 \\ Q_{12}^{(m)} & Q_{22}^{(m)} & 0 \\ 0 & 0 & Q_{66}^{(m)} \end{bmatrix},$$

$$\mathbf{Q}_\zeta^{(m)} = \begin{bmatrix} \left(c_{13}^{(m)}/c_{33}^{(m)}\right) \\ \left(c_{23}^{(m)}/c_{33}^{(m)}\right) \\ 0 \end{bmatrix},$$

$$\mathbf{B}_1^{(m)} = \begin{bmatrix} \left(\psi_u^{(m)}\right)_i \partial_x & 0 \\ 0 & \left(\psi_u^{(m)}\right)_i \partial_y \\ \left(\psi_u^{(m)}\right)_i \partial_y & \left(\psi_u^{(m)}\right)_i \partial_x \end{bmatrix}_{i=1,2,\cdots,N_u+1}, \quad \mathbf{B}_2^{(m)} = \left[\left(\psi_\sigma^{(m)}\right)_i \right]_{i=1,2,\cdots,N_\sigma+1},$$

$$\mathbf{B}_3^{(m)} = \begin{bmatrix} \left(D\psi_u^{(m)}\right)_i & 0 \\ 0 & \left(D\psi_u^{(m)}\right)_i \end{bmatrix}_{i=1,2,\cdots,N_u+1}, \quad \mathbf{B}_4^{(m)} = \begin{bmatrix} \left(\psi_w^{(m)}\right)_i \partial_x \\ \left(\psi_w^{(m)}\right)_i \partial_y \end{bmatrix}_{i=1,2,\cdots,N_w+1},$$

$$\mathbf{B}_5^{(m)} = \begin{bmatrix} \left(\psi_\tau^{(m)}\right)_i & 0 \\ 0 & \left(\psi_\tau^{(m)}\right)_i \end{bmatrix}_{i=1,2,\cdots,N_\tau+1}, \quad \mathbf{B}_6^{(m)} = \left[\left(D\psi_w^{(m)}\right)_i \right]_{i=1,2,\cdots,N_w+1},$$

$$\mathbf{B}_7^{(m)} = \begin{bmatrix} \left(\psi_u^{(m)}\right)_i & 0 \\ 0 & \left(\psi_u^{(m)}\right)_i \end{bmatrix}_{i=1,2,\cdots,N_u+1}, \quad \mathbf{B}_8^{(m)} = \left[\left(\psi_w^{(m)}\right)_i \right]_{i=1,2,\cdots,N_w+1};$$

and the superscript of T denotes the transpose of the matrices or vectors; and Γ_u and Γ_σ stand for the boundary edges, in which the essential and natural conditions are prescribed.

2.3 The system motion equations of RMVT-based FLMs

The free vibration of simply-supported, multilayered composite and FGM plates is studied in the following illustrative examples, where the tractions on the lateral surfaces of the plate are free and given as

$$\left[\tau_{x\zeta}^{(N)} \quad \tau_{y\zeta}^{(N)} \quad \sigma_{\zeta}^{(N)}\right] = [0 \quad 0 \quad 0] \qquad on \qquad z_N = h_N/2 \quad (\text{or } \zeta = -h/2)\,. \tag{16a}$$

$$\left[\tau_{x\zeta}^{(1)} \quad \tau_{y\zeta}^{(1)} \quad \sigma_{\zeta}^{(1)}\right] = [0 \quad 0 \quad 0] \qquad on \qquad z_1 = h_1/2 \quad (\text{or } \zeta = -h/2)\,. \tag{16b}$$

The edge boundary conditions of each individual layer are considered as fully simple supports, which requires that the following quantities are satisfied.

$$u_y^{(m)} = u_\zeta^{(m)} = \sigma_x^{(m)} = 0, \text{ at } x = 0,\ x = L_x \text{ and } m = 1, 2, \cdots, N; \tag{17a}$$

$$u_x^{(m)} = u_\zeta^{(m)} = \sigma_y^{(m)} = 0, \text{ at } y = 0,\ y = L_y \text{ and } m = 1, 2, \cdots, N. \tag{17b}$$

By means of the separation of variables, the primary field variables of each individual layer are expanded as the following forms of a double Fourier series so that the boundary conditions of the simply supported edges are exactly satisfied. They are given as

$$\left(u_x^{(m)},\ \tau_{x\zeta}^{(m)}\right) = \sum_{\hat{m}=1}^{\infty}\sum_{\hat{n}=1}^{\infty}\left(u_{\hat{m}\hat{n}}^{(m)},\ \tau_{13\hat{m}\hat{n}}^{(m)}\right)\ \cos(\tilde{m}x)\ \sin(\tilde{n}y)\ e^{i\omega t}, \tag{18}$$

$$\left(u_y^{(m)},\ \tau_{y\zeta}^{(m)}\right) = \sum_{\hat{m}=1}^{\infty}\sum_{\hat{n}=1}^{\infty}\left(v_{\hat{m}\hat{n}}^{(m)},\ \tau_{23\hat{m}\hat{n}}^{(m)}\right)\ \sin(\tilde{m}x)\ \cos(\tilde{n}y)\ e^{i\omega t}, \tag{19}$$

$$\left(u_\zeta^{(m)},\ \sigma_{\zeta}^{(m)}\right) = \sum_{\hat{m}=1}^{\infty}\sum_{\hat{n}=1}^{\infty}\left(w_{\hat{m}\hat{n}}^{(m)},\ \sigma_{13\hat{m}\hat{n}}^{(m)}\right)\ \sin(\tilde{m}x)\ \sin(\tilde{n}y)\ e^{i\omega t}, \tag{20}$$

where ω denotes the frequency of the natural vibration of the plate; $\tilde{m} = \hat{m}\pi/L_x$, $\tilde{n} = \hat{n}\pi/L_y$; and $\hat{m}$ and $\hat{n}$ are positive integers.

After introducing Eqs. (18)–(20) in Eq. (15) and applying the MRVT-based Hamilton principle, which is $\delta\Pi_R = 0$, we obtain the system motion equations of the plate

as follows:

$$\sum_{m=1}^{N}\left\{\left(-\omega^2\right)\begin{bmatrix}\mathbf{M}_{\mathbf{I\ I}}^{(m)} & \mathbf{0} & \mathbf{0} & \mathbf{0}\\ \mathbf{0} & \mathbf{M}_{\mathbf{II\ II}}^{(m)} & \mathbf{0} & \mathbf{0}\\ \mathbf{0} & \mathbf{0} & \mathbf{0} & \mathbf{0}\\ \mathbf{0} & \mathbf{0} & \mathbf{0} & \mathbf{0}\end{bmatrix}+\begin{bmatrix}\mathbf{K}_{\mathrm{I\ I}}^{(m)} & \mathbf{K}_{\mathrm{I\ II}}^{(m)} & \mathbf{K}_{\mathrm{I\ III}}^{(m)} & \mathbf{K}_{\mathrm{I\ IV}}^{(m)}\\ \mathbf{K}_{\mathrm{II\ I}}^{(m)} & \mathbf{K}_{\mathrm{II\ II}}^{(m)} & \mathbf{K}_{\mathrm{II\ III}}^{(m)} & \mathbf{K}_{\mathrm{II\ IV}}^{(m)}\\ \mathbf{K}_{\mathrm{III\ I}}^{(m)} & \mathbf{K}_{\mathrm{III\ II}}^{(m)} & \mathbf{K}_{\mathrm{III\ III}}^{(m)} & \mathbf{K}_{\mathrm{III\ IV}}^{(m)}\\ \mathbf{K}_{\mathrm{IV\ I}}^{(m)} & \mathbf{K}_{\mathrm{IV\ II}}^{(m)} & \mathbf{K}_{\mathbf{IV\ III}}^{(m)} & \mathbf{K}_{\mathrm{IV\ IV}}^{(m)}\end{bmatrix}\right\}\begin{bmatrix}\tilde{\mathbf{u}}^{(m)}\\ \tilde{\mathbf{w}}^{(m)}\\ \tilde{\tau}^{(m)}\\ \tilde{\sigma}^{(m)}\end{bmatrix}=\begin{bmatrix}\mathbf{0}\\ \mathbf{0}\\ \mathbf{0}\\ \mathbf{0}\end{bmatrix}, \quad (21)$$

where $\mathbf{K}_{i\ j}^{(m)}=\left(\mathbf{K}_{j\ i}^{(m)}\right)^T$ $(i,j=\mathbf{I},\ \mathbf{II},\ \mathbf{III},\ \mathbf{IV})$;

$$\mathbf{K}_{\mathbf{I\ I}}^{(m)}=\int_{-h_m/2}^{h_m/2}\left(\tilde{\mathbf{B}}_1^{(m)}\right)^T\mathbf{Q}_p^{(m)}\tilde{\mathbf{B}}_1^{(m)}\,dz_m,$$

$$\mathbf{K}_{\mathbf{I\ II}}^{(m)}=\mathbf{K}_{\mathbf{II\ I}}^{(\mathbf{m})}=\mathbf{K}_{\mathbf{II\ II}}^{(\mathbf{m})}=\mathbf{0},\quad \mathbf{K}_{\mathbf{I\ III}}^{(m)}=\int_{-h_m/2}^{h_m/2}\left(\mathbf{B}_3^{(m)}\right)^T\mathbf{B}_5^{(m)}\,dz_m,$$

$$\mathbf{K}_{\mathbf{I\ IV}}^{(m)}=\int_{-h_m/2}^{h_m/2}\left(\tilde{\mathbf{B}}_1^{(m)}\right)^T\mathbf{Q}_\zeta^{(m)}\mathbf{B}_2^{(m)}\,dz_m,\quad \mathbf{K}_{\mathbf{II\ III}}^{(m)}=\int_{-h_m/2}^{h_m/2}\left(\tilde{\mathbf{B}}_4^{(m)}\right)^T\mathbf{B}_5^{(m)}\,dz_m$$

$$\mathbf{K}_{\mathbf{II\ IV}}^{(m)}=\int_{-h_m/2}^{h_m/2}\left(\mathbf{B}_6^{(m)}\right)^T\mathbf{B}_2^{(m)}\,dz_m,\quad \mathbf{K}_{\mathbf{III\ III}}^{(m)}=\int_{-h_m/2}^{h_m/2}\left(\mathbf{B}_5^{(m)}\right)^T\mathbf{S}^{(m)}\mathbf{B}_5^{(m)}\,dz_m$$

$$\mathbf{K}_{\mathbf{IV\ IV}}^{(m)}=\int_{-h_m/2}^{h_m/2}\left(1/c_{33}^{(m)}\right)\left(\mathbf{B}_2^{(m)}\right)^T\mathbf{B}_2^{(m)}\,dz_m,$$

$$\mathbf{M}_{\mathbf{I\ I}}^{(m)}=\int_{-h_m/2}^{h_m/2}\rho\left(\mathbf{B}_7^{(m)}\right)^T\mathbf{B}_7^{(m)}\,dz_m,\quad \mathbf{M}_{\mathbf{II\ II}}^{(m)}=\int_{-h_m/2}^{h_m/2}\rho\left(\mathbf{B}_8^{(m)}\right)^T\mathbf{B}_8^{(m)}\,dz_m,$$

$$\tilde{\mathbf{B}}_1^{(m)}=\begin{bmatrix}-\tilde{m}\left(\psi_u^{(m)}\right)_i & 0\\ 0 & -\tilde{n}\left(\psi_u^{(m)}\right)_i\\ \tilde{n}\left(\psi_u^{(m)}\right)_i & \tilde{m}\left(\psi_u^{(m)}\right)_i\end{bmatrix}_{i=1,2,\cdots,N_u+1},$$

$$\tilde{\mathbf{B}}_4^{(m)} = \left[\begin{matrix} \tilde{m}\left(\psi_w^{(m)}\right)_i \\ \tilde{n}\left(\psi_w^{(m)}\right)_i \end{matrix}\right]_{i=1,2,\cdots,N_w+1} ;$$

and

$$\tilde{\mathbf{u}}^{(m)} = \left[\begin{matrix} \left(u_{\hat{m}\hat{n}}^{(m)}\right)_i \\ \left(v_{\hat{m}\hat{n}}^{(m)}\right)_i \end{matrix}\right]_{i=1,2,\cdots,N_u+1}, \quad \tilde{\mathbf{w}}^{(m)} = \left[\left(w_{\hat{m}\hat{n}}^{(m)}\right)_i\right]_{i=1,2,\cdots,N_w+1},$$

$$\tilde{\boldsymbol{\tau}}^{(m)} = \left[\begin{matrix} \left(\tau_{13\hat{m}\hat{n}}^{(m)}\right)_l \\ \left(\tau_{23\hat{m}\hat{n}}^{(m)}\right)_l \end{matrix}\right]_{i=1,2,\cdots,N_\tau+1}, \quad \tilde{\boldsymbol{\sigma}}^{(m)} = \left[\left(\sigma_{3\hat{m}\hat{n}}^{(m)}\right)_i\right]_{i=1,2,\cdots,N_\sigma+1}.$$

It is noted that the determination of the local mass and stiffness sub-matrices derived and given in Eq. (21), requires an integration evaluation, in which the integrands are the multiplication of the related shaped functions and thickness-dependent material properties. A numerical integration technique, the Gaussian quadrature commonly used in the FEMs, is used to evaluate these local stiffness sub-matrices. To achieve this, we construct a background integration mesh in the thickness coordinate for each individual layer, in which it is further divided into N_l integration layers and the N_g-term Gaussian quadrature formula is applied to each integration layer. The implementation of the present FLMs shows that using a 20-layer integration mesh ($N_l = 20$) with seven-term Gaussian quadrature formula (N_g=7) may evaluate each integration to five-decimal accuracy, and this is adopted for the later work of the present analysis.

After using Eq. (21) and assembling the local mass and stiffness sub-matrices of each layer constituting the plate by following the standard process of the FEMs, in which the displacement and transverse stress continuity conditions at the interfaces between adjacent layers are imposed and thus satisfied a priori for these RMVT-based FLMs, we may construct the global mass and stiffness matrices for the plate, which are given as

$$\left\{ (-\omega^2) \begin{bmatrix} \mathbf{M}_{11} & \mathbf{0} & \mathbf{0} & \mathbf{0} \\ \mathbf{0} & \mathbf{M}_{22} & \mathbf{0} & \mathbf{0} \\ \mathbf{0} & \mathbf{0} & \mathbf{0} & \mathbf{0} \\ \mathbf{0} & \mathbf{0} & \mathbf{0} & \mathbf{0} \end{bmatrix} + \begin{bmatrix} \mathbf{K_{11}} & \mathbf{0} & \mathbf{K_{13}} & \mathbf{K_{14}} \\ \mathbf{0} & \mathbf{0} & \mathbf{K_{23}} & \mathbf{K_{24}} \\ \mathbf{K_{31}} & \mathbf{K_{32}} & \mathbf{K_{33}} & \mathbf{0} \\ \mathbf{K_{41}} & \mathbf{K_{42}} & \mathbf{0} & \mathbf{K_{44}} \end{bmatrix} \right\} \begin{bmatrix} \mathbf{u} \\ \mathbf{w} \\ \tau \\ \sigma \end{bmatrix} = \begin{bmatrix} \mathbf{0} \\ \mathbf{0} \\ \mathbf{0} \\ \mathbf{0} \end{bmatrix}. \quad (22)$$

From the last two equations in Eq. (22), we obtain

$$\begin{bmatrix} \tau \\ \sigma \end{bmatrix} = - \begin{bmatrix} \mathbf{K_{33}} & \mathbf{0} \\ \mathbf{0} & \mathbf{K_{44}} \end{bmatrix}^{-1} \begin{bmatrix} \mathbf{K_{31}} & \mathbf{K_{32}} \\ \mathbf{K_{41}} & \mathbf{K_{42}} \end{bmatrix} \begin{bmatrix} \mathbf{u} \\ \mathbf{w} \end{bmatrix}. \quad (23)$$

Using Eq. (23), Eq. (22) can be condensed in the following form

$$\left\{ \begin{bmatrix} \mathbf{K_{11}} - \omega^2 \mathbf{M_{11}} & \mathbf{0} \\ \mathbf{0} & -\omega^2 \mathbf{M_{22}} \end{bmatrix} - \begin{bmatrix} \mathbf{K_{13}} & \mathbf{K_{14}} \\ \mathbf{K_{23}} & \mathbf{K_{24}} \end{bmatrix} \begin{bmatrix} \mathbf{K_{33}} & \mathbf{0} \\ \mathbf{0} & \mathbf{K_{44}} \end{bmatrix}^{-1} \begin{bmatrix} \mathbf{K_{31}} & \mathbf{K_{32}} \\ \mathbf{K_{41}} & \mathbf{K_{42}} \end{bmatrix} \right\} \begin{bmatrix} \mathbf{u} \\ \mathbf{w} \end{bmatrix} = \begin{bmatrix} \mathbf{0} \\ \mathbf{0} \end{bmatrix}. \quad (24)$$

Equation (24) represents a standard eigenvalue problem, and a nontrivial solution of this exists if the determinant of the coefficient matrix vanishes. Thus, the natural frequencies of the plate for a set of fixed values $(\hat{m},\ \hat{n})$ can be obtained by

$$\left| \begin{bmatrix} \mathbf{K_{11}} - \omega^2 \mathbf{M_{11}} & \mathbf{0} \\ \mathbf{0} & -\omega^2 \mathbf{M_{22}} \end{bmatrix} - \begin{bmatrix} \mathbf{K_{13}} & \mathbf{K_{14}} \\ \mathbf{K_{23}} & \mathbf{K_{24}} \end{bmatrix} \begin{bmatrix} \mathbf{K_{33}} & \mathbf{0} \\ \mathbf{0} & \mathbf{K_{44}} \end{bmatrix}^{-1} \begin{bmatrix} \mathbf{K_{31}} & \mathbf{K_{32}} \\ \mathbf{K_{41}} & \mathbf{K_{42}} \end{bmatrix} \right| = 0. \quad (25)$$

Once Eq. (25) is solved, the eigenvalues and their corresponding eigenvectors, which are the natural frequencies and modal displacements at each nodal plane, respectively, can be obtained. Subsequently, the modal transverse stresses at each nodal plane can be determined using Eq. (23), while the modal in-plane stresses at the nodal planes can be obtained using Hooke's law, and are given by

$$\left(\sigma_x^{(m)},\ \sigma_y^{(m)}\right) = \sum_{\hat{m}=1}^{\infty} \sum_{\hat{n}=1}^{\infty} \left(\sigma_{1\hat{m}\hat{n}}^{(m)},\ \sigma_{2\hat{m}\hat{n}}^{(m)}\right) \sin(\tilde{m}x)\ \sin(\tilde{n}y)\ e^{i\omega t}, \quad (26)$$

$$\tau_{xy}^{(m)} = \sum_{\hat{m}=1}^{\infty} \sum_{\hat{n}=1}^{\infty} \tau_{12\hat{m}\hat{n}}^{(m)}\ \cos(\tilde{m}x)\ \cos(\tilde{n}y)\ e^{i\omega t}, \quad (27)$$

where $\left[\sigma_{1\hat{m}\hat{n}}^{(m)} \quad \sigma_{2\hat{m}\hat{n}}^{(m)} \quad \tau_{12\hat{m}\hat{n}}^{(m)}\right]^T = \mathbf{Q}_p^{(m)} \tilde{\mathbf{B}}_1^{(m)} \tilde{\mathbf{u}}^{(m)} + \mathbf{Q}_\zeta^{(m)} \mathbf{B}_2^{(m)} \tilde{\sigma}^{(m)}$.

Using this unified formulation of RMVT-based FLMs, we may analyze the quasi-3D free vibration of multilayered composite and FGM plates, and the performances of various RMVT-based FLMs with different orders used for the expansion of the in-plane and out-of-plane displacements and transverse shear and normal stresses can also be studied.

3 PVD-based finite layer methods

3.1 The Hamilton principle

The Hamilton principle is a displacement-based energy principle, in which only the displacement components are regarded as the primary variables, as given in Eqs.

(1)–(3). The Hamilton principle is used to derive the system motion equations of the plate for the PVD-based FLMs, and its corresponding energy functional for the plate is written in the form of

$$I = \int_{t_1}^{t_2} (T - V)\, dt, \tag{28}$$

where the kinetic energy T is in the same form as given in Eq. (14), while V denotes the potential energy of the plate, and is given as

$$\begin{aligned} V = \tfrac{1}{2} \sum_{m=1}^{N} \int_{-h_m/2}^{h_{km}/2} \iint_{\Omega} \Big[& \sigma_x^{(m)} \varepsilon_x^{(m)} + \sigma_y^{(m)} \varepsilon_y^{(m)} + \sigma_\zeta^{(m)} \varepsilon_\zeta^{(m)} + \tau_{x\zeta}^{(m)} \gamma_{x\zeta}^{(m)} \\ & + \tau_{y\zeta}^{(m)} \gamma_{y\zeta}^{(m)} + \tau_{xy}^{(m)} \gamma_{xy}^{(m)} \Big]\, dx\, dy\, dz_m \\ & - \sum_{m=1}^{N} \int_{-h_m/2}^{h_m/2} \int_{\Gamma_\sigma} \left[\bar{t}_x^{(m)}\ u_x^{(m)} + \bar{t}_y^{(m)}\ u_y^{(m)} + \bar{t}_\zeta^{(m)}\ u_\zeta^{(m)} \right] d\Gamma\, dz_m. \end{aligned}$$

For an N-layered plate with heterogeneous material properties for each individual layer, only the displacement components are subject to variation. By using the kinematic assumptions given in Eqs. (1)–(3), we may express the first-order variation of the energy functional I as follows:

$$\delta I = \int_{t_1}^{t_2} (\delta T - \delta V)\, dt, \tag{29}$$

where δT was given in Eq. (15), and

$$\begin{aligned} \delta V = & \iint_{\Omega} \sum_{m=1}^{N} \int_{-h_m/2}^{h_m/2} \left[\left(\delta \varepsilon_p^{(m)} \right)^T \sigma_p^{(m)} + \left(\delta \varepsilon_s^{(m)} \right)^T \sigma_s^{(m)} + \delta \varepsilon_\zeta\, \sigma_\zeta^{(m)} \right] dx\, dy\, dz_m \\ & - \sum_{m=1}^{N} \int_{-h_m/2}^{h_m/2} \int_{\Gamma_\sigma} \left[\bar{t}_x^{(m)}\ \delta u_x^{(m)} + \bar{t}_y^{(m)}\ \delta u_y^{(m)} + \bar{t}_\zeta^{(m)}\ \delta u_\zeta^{(m)} \right] d\Gamma\, dz_m, \end{aligned}$$

in which $\varepsilon_p^{(m)}$, $\varepsilon_s^{(m)}$ and $\varepsilon_\zeta^{(m)}$ are in the same forms as those given in Eq. (15), and

$$\sigma_p^{(m)} = \mathbf{C}_p^{(m)} \mathbf{B}_1^{(m)} \mathbf{u}^{(m)} + \mathbf{C}_\zeta^{(m)} \mathbf{B}_6^{(m)} \mathbf{w}^{(m)},$$

$$\sigma_s^{(m)} = \mathbf{C}^{(m)} \mathbf{B}_3^{(m)} \mathbf{u}^{(m)} + \mathbf{C}^{(m)} \mathbf{B}_4^{(m)} \mathbf{w}^{(m)},$$

$$\sigma_\zeta^{(m)} = \mathbf{C}_\zeta^{(m)} \mathbf{B}_1^{(m)} \mathbf{u}^{(m)} + c_{33}^{(m)} \mathbf{B}_6^{(m)} \mathbf{w}^{(m)},$$

$$\mathbf{C}_p^{(m)} = \begin{bmatrix} c_{11}^{(m)} & c_{12}^{(m)} & 0 \\ c_{12}^{(m)} & c_{22}^{(m)} & 0 \\ 0 & 0 & c_{66}^{(m)} \end{bmatrix}, \quad \mathbf{C}_\zeta^{(m)} = \begin{bmatrix} c_{13}^{(m)} \\ c_{23}^{(m)} \\ 0 \end{bmatrix}, \quad \mathbf{C}^{(m)} = \begin{bmatrix} c_{55}^{(m)} & 0 \\ 0 & c_{44}^{(m)} \end{bmatrix}.$$

3.2 The system motion equations of PVD-based FLMs

After introducing Eqs. (18)–(20) in Eq. (29) and applying Hamilton's principle, which is $\delta I = 0$, we obtain the system motion equations of the plate as follows:

$$\sum_{m=1}^{N} \left\{ (-\omega^2) \begin{bmatrix} \mathbf{M}_{\mathrm{I\ I}}^{(m)} & \mathbf{0} \\ \mathbf{0} & \mathbf{M}_{\mathrm{II\ II}}^{(m)} \end{bmatrix} + \begin{bmatrix} \mathbf{D}_{\mathrm{I\ I}}^{(m)} & \mathbf{D}_{\mathrm{I\ II}}^{(m)} \\ \mathbf{D}_{\mathrm{II\ I}}^{(m)} & \mathbf{D}_{\mathrm{II\ II}}^{(m)} \end{bmatrix} \right\} \begin{bmatrix} \tilde{\mathbf{u}}^{(m)} \\ \tilde{\mathbf{w}}^{(m)} \end{bmatrix} = \begin{bmatrix} \mathbf{0} \\ \mathbf{0} \end{bmatrix}, \tag{30}$$

where $\mathbf{M}_{\mathbf{I\ I}}^{(m)}$ and $\mathbf{M}_{\mathbf{II\ II}}^{(m)}$ are in the same forms as those given in Eq. (21); $\mathbf{D}_{i\ j}^{(m)} = \left(\mathbf{D}_{j\ i}^{(m)}\right)^T$ $(i, j = \mathbf{I}, \mathbf{II})$,

$$\mathbf{D}_{\mathbf{I\ I}}^{(m)} = \int_{-h_m/2}^{h_m/2} \left[\left(\tilde{\mathbf{B}}_1^{(m)}\right)^T \mathbf{C}_p^{(m)} \tilde{\mathbf{B}}_1^{(m)} + \left(\mathbf{B}_3^{(m)}\right)^T \mathbf{C}^{(m)} \mathbf{B}_3^{(m)} \right] dz_m,$$

$$\mathbf{D}_{\mathbf{I\ II}}^{(m)} = \int_{-h_m/2}^{h_m/2} \left[\left(\tilde{\mathbf{B}}_1^{(m)}\right)^T \mathbf{C}_\zeta^{(m)} \mathbf{B}_6^{(m)} + \left(\mathbf{B}_3^{(m)}\right)^T \mathbf{C}^{(m)} \tilde{\mathbf{B}}_4^{(m)} \right] dz_m,$$

$$\mathbf{D}_{\mathbf{II\ II}}^{(m)} = \int_{-h_m/2}^{h_m/2} \left[\left(\tilde{\mathbf{B}}_4^{(m)}\right)^T \mathbf{C}^{(m)} \tilde{\mathbf{B}}_4^{(m)} + \left(\mathbf{B}_6^{(m)}\right)^T (c_{33}^{(m)}) \mathbf{B}_6^{(m)} \right] dz_m.$$

Again, after using Eq. (30) and assembling the local mass and stiffness submatrices of each layer constituting the plate by following the standard process of the FEMs, in which the displacement continuity conditions, not including the transverse stress ones, at the interfaces between adjacent layers are imposed, we may construct the global mass and stiffness matrices for the plate, which are given as

$$\left\{ (-\omega^2) \begin{bmatrix} \mathbf{M}_{11} & \mathbf{0} \\ \mathbf{0} & \mathbf{M}_{22} \end{bmatrix} + \begin{bmatrix} \mathbf{D}_{11} & \mathbf{D}_{12} \\ \mathbf{D}_{21} & \mathbf{D}_{22} \end{bmatrix} \right\} \begin{bmatrix} \mathbf{u} \\ \mathbf{w} \end{bmatrix} = \begin{bmatrix} \mathbf{0} \\ \mathbf{0} \end{bmatrix}. \tag{31}$$

Equation (31) represents a standard eigenvalue problem, and a nontrivial solution to this exists if the determinant of the coefficient matrix vanishes. Thus, the natural

frequencies of the plate for a set of fixed values $(\hat{m}, \quad \hat{n})$ can be obtained by

$$\left| \begin{bmatrix} \mathbf{D_{11}} - \omega^2 \mathbf{M_{11}} & \mathbf{D_{12}} \\ \mathbf{D_{21}} & \mathbf{D_{22}} - \omega^2 \mathbf{M_{22}} \end{bmatrix} \right| = 0. \tag{32}$$

Once Eq. (32) is solved, the eigenvalues and their corresponding eigenvectors, which are the natural frequencies and modal displacements at each nodal plane, respectively, can be obtained. Subsequently, the modal transverse stresses at each nodal plane can be determined using Hooke's law, and these are obtained as the same forms given in Eqs. (26)–(27) and the second terms of Eqs. (18)–(20), in which

$$\left[\sigma_{1\hat{m}\hat{n}}^{(m)} \quad \sigma_{2\hat{m}\hat{n}}^{(m)} \quad \tau_{12\hat{m}\hat{n}}^{(m)} \right]^T = \mathbf{C}_p^{(m)} \tilde{\mathbf{B}}_1^{(m)} \tilde{\mathbf{u}}^{(m)} + \mathbf{C}_\zeta^{(m)} \mathbf{B}_6^{(m)} \tilde{w}^{(m)}, \tag{33}$$

$$\left[\tau_{13\hat{m}\hat{n}}^{(m)} \quad \tau_{23\hat{m}\hat{n}}^{(m)} \right] = \mathbf{C}^{(m)} \mathbf{B}_3^{(m)} \tilde{\mathbf{u}}^{(m)} + \mathbf{C}^{(m)} \mathbf{B}_4^{(m)} \tilde{\mathbf{w}}^{(m)}, \tag{34}$$

$$\sigma_{3\hat{m}\hat{n}}^{(m)} = \mathbf{C}_\zeta^{(m)} \tilde{\mathbf{B}}_1^{(m)} \tilde{\mathbf{u}}^{(m)} + c_{33}^{(m)} \mathbf{B}_6^{(m)} \tilde{\mathbf{w}}^{(m)}. \tag{35}$$

As we mentioned above, the transverse stresses in Eqs. (34)–(35) are calculated using Hooke's law, and this might lead to the poor predictions for those. However, an integration approach derived from the dynamic stress equilibrium equations, is recommended instead of this in the literature, and is given as

$$\tau_{13\hat{m}\hat{n}}^{(m)} = \left(\tau_{13\hat{m}\hat{n}}^{(m-1)} \right)_{N_\tau+1} + \int_{-h_m/2}^{z_m} \left(-\tilde{m} \sigma_{1\hat{m}\hat{n}}^{(m)} + \tilde{n} \tau_{12\hat{m}\hat{n}}^{(m)} - \rho \, \omega^2 \, u_{\hat{m}\hat{n}}^{(m)} \right) dz_m \, , \tag{36}$$

$$\tau_{23\hat{m}\hat{n}}^{(m)} = \left(\tau_{23\hat{m}\hat{n}}^{(m-1)} \right)_{N_\tau+1} + \int_{-h_m/2}^{z_m} \left(\tilde{m} \, \tau_{12\hat{m}\hat{n}}^{(m)} - \tilde{n} \, \sigma_{2\hat{m}\hat{n}}^{(m)} - \rho \, \omega^2 \, v_{\hat{m}\hat{n}}^{(m)} \right) dz_m \, , \tag{37}$$

$$\sigma_{3\hat{m}\hat{n}}^{(m)} = \left(\sigma_{3\hat{m}\hat{n}}^{(m-1)} \right)_{N_\sigma+1} + \int_{-h_m/2}^{z_m} \left(\tilde{m} \tau_{13\hat{m}\hat{n}}^{(m)} + \tilde{n} \tau_{23\hat{m}\hat{n}}^{(m)} - \rho \, \omega^2 \, w_{\hat{m}\hat{n}}^{(m)} \right) dz_m \, . \tag{38}$$

Using this unified formulation for PVD-based FLMs, we may analyze the 3D free vibration of multilayered composite and FGM plates, and the performances of various PVD-based FLMs with different orders used for the expansion of the in-plane and out-of-plane displacements can also be studied.

4 Illustrative examples

Because the unified formulations of RMVT- and PVD-based FLMs for the free vibration analysis of laminated composite and FGM plates were presented above, various combinations of the orders used for expansion of displacements and transverse stresses can also be freely chosen. Hence, the acronym of $\mathrm{LD}_{N_u N_w}$ is used

to represent various PVD-based FLMs, in which the in- and out-of-plane displacements are expanded as the N_u- and N_w-order Lagrange polynomials in the thickness coordinate of each layer, respectively, while that of $\mathrm{LM}_{N_u\,N_w}^{N_\tau\,N_\sigma}$ is defined to represent various RMVT-based FLMs, in which the in- and out-of-plane displacements are expanded as the N_u- and N_w-order Lagrange polynomials, respectively, and the transverse shear and normal stresses are expanded as the N_τ- and N_σ-order Lagrange polynomials in the thickness coordinate of each layer, respectively. In addition, because an *h*-refinement process is adopted for this analysis, the values of N_i $(i = u,\ v,\ \tau$ and $\sigma)$ are taken to be 1 or 2 in the following examples.

4.1 Laminated composite plates

Dynamic-version of Demasi's test case 1

Test case 1 in Demasi (2009e) considers the static behavior of laminated composite and FGM plates subject to mechanical loads applied on the top surface of the plate, and was used to examine the so-called numerical instability resulting from the relative orders used for the expansion of the stresses and displacements, for the earlier GUF (Demasi, 2009e) and the RMVT- and PVD-based FLMs (Wu and Li, 2010b). In this dynamic-version of Demasi's test case 1, the free vibration of the simply supported, two-layered composite elastic plates (i.e., $\left[0^0/90^0\right]$, in which the 0^0 and 90^0 layers are the bottom and top layers, respectively) is studied. The geometric parameters of the plates are taken to be $L_x/L_y = 1$, and $S = L_x/h$=2, 5, 10, 20, 50 and 100; a frequency parameter is defined as $\Omega = \left(\omega L_x^2/h\right)\sqrt{\rho/E_{22}}$; and the material properties of the top and bottom layers are identical to those used in Demasi (2009e), and given as follows:

For the 0^0 layer (the bottom layer),

$$E_{11}/E_{22} = 25, \quad E_{11}/E_{33} = 25, \quad E_{11}/G_{12} = 50,$$

$$E_{11}/G_{13} = 50, \quad E_{11}/G_{23} = 125,$$

$$\upsilon_{12} = \upsilon_{13} = \upsilon_{23} = 0.25, \quad E_{22} = 1.0\text{x}10^6\,\text{psi (or } 6.89\text{ GPa)}. \tag{39}$$

For the 90^0 layer (the top layer),

$$E_{11}/E_{22} = 25, \quad E_{11}/E_{33} = 25/10, \quad E_{11}/G_{12} = 50,$$

$$E_{11}/G_{13} = 50, \quad E_{11}/G_{23} = 125,$$

$$\upsilon_{12} = \upsilon_{13} = \upsilon_{23} = 0.25, \quad E_{22} = 1.0\text{x}10^6\,\text{psi (or } 6.89\text{ GPa)}. \tag{40}$$

where the subscript 1 denotes the direction parallel to the fiber directions, and 2 and 3 transverse to the fiber direction.

Table 1 shows the fundamental frequency parameters of the plates with different values of the length-to-thickness ratio (S=L_x/h) using various RMVT- and PVD-based FLMs with an h-refinement process, in which the plate is divided into numerous equal-thickness layers, such as N=2, 4 and 8. In Table 1, the present solutions are compared with the 3D exact solutions obtained using the modified Pagano method (Wu and Lü, 2009) to evaluate the accuracy and convergence rate of various RMVT- and PVD- based FLMs, and we find that $\mathrm{LD}_{22} > \mathrm{LD}_{21} > \mathrm{LD}_{11}$, $\mathrm{LM}_{22}^{22} > \mathrm{LM}_{21}^{21} > \mathrm{LM}_{21}^{22} > \mathrm{LM}_{11}^{11}$, and the symbol "$>$" means the solutions of the former are more accurate than those of the latter, and the convergence rate of the former is faster than that of the latter. In order to have a clearer picture with regard to the dynamic response performance of the FLMs presented in this work, we show the through-thickness distributions of modal displacement and stress components of a thick square plate ($S = 4$) obtained using the present PVD-based ones (LD_{21} and LD_{22}) in Figs. 2–3 and RMVT-based ones (LM_{21}^{21}, LM_{21}^{22} and LM_{22}^{22}) in Figs. 5–7, in which the modal stress components are determined using Hooke's law and the interpolation functions a priori, respectively. It is seen in Figs. 2–3 that PVD-based FLMs yield good predictions for the modal in-plane stresses and displacements, while they yield poor predictions for the modal transverse stresses using Hooke's Law, especially for the modal transverse normal stress. In addition, and even worse, they yield two values at the interfaces between adjacent layers due to the sudden changes of the material properties, violating the requirements of 3D elasticity. In view of the poor predictions obtained using Hooke's law, an integration approach derived from the dynamic stress equilibrium equations is thus recommended. Fig. 4 shows the through-thickness distributions of the modal transverse stresses of LD_{21} and LD_{22}, which are obtained using the integration approach. It is seen in Fig. 4 that the accuracy for the modal transverse stresses is much improved, and that the eight-layer solutions of LD_{22} are in excellent agreement with the 3D exact solutions obtained using the modified Pagano method (Wu and Lü, 2009). It is seen in Figs. 5 and 7 that the solutions of LM_{21}^{21} and LM_{22}^{22} smoothly vary through the thickness coordinate, and they are numerically stable; and the eight-layer solutions of these two FLMs are in excellent agreement with the 3D exact solutions, and the rate of convergence of LM_{22}^{22} for the modal transverse normal stress is faster than that of LM_{21}^{21}. It is observed from Figs. 6 (e, f) that the solutions of through-thickness distributions of modal transverse normal stress obtained using the interpolation functions a priori in LM_{21}^{22} oscillate in the top layer, and the LM_{21}^{22} theory fails to yield the satisfactory predictions for these. This observation supports Demasi's conclusions on the numerical instability of RMVT-based theories (Demasi, 2009e) in the static cases, that is there is no numerical instability if the order of out-of-plane displacement (u_ζ) is the same as that of transverse normal stress (σ_ζ), otherwise, numerical instability will occur.

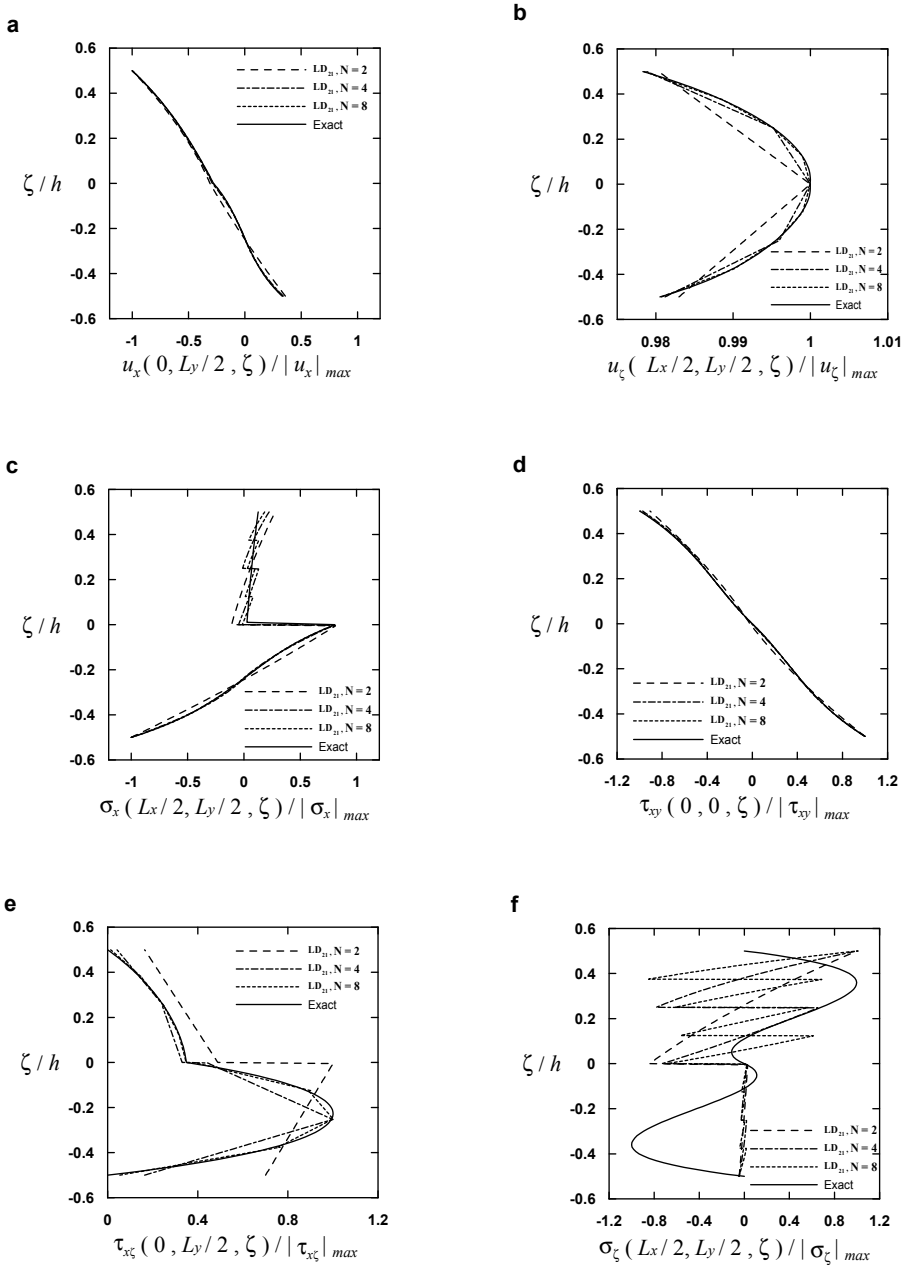

Figure 2: The through-thickness distributions of various modal field variables in a $\left[0^0/90^0\right]$ laminate obtained using the present LD_{21} with N=2, 4, 8 (Dynamic version of Demasi's test case 1).

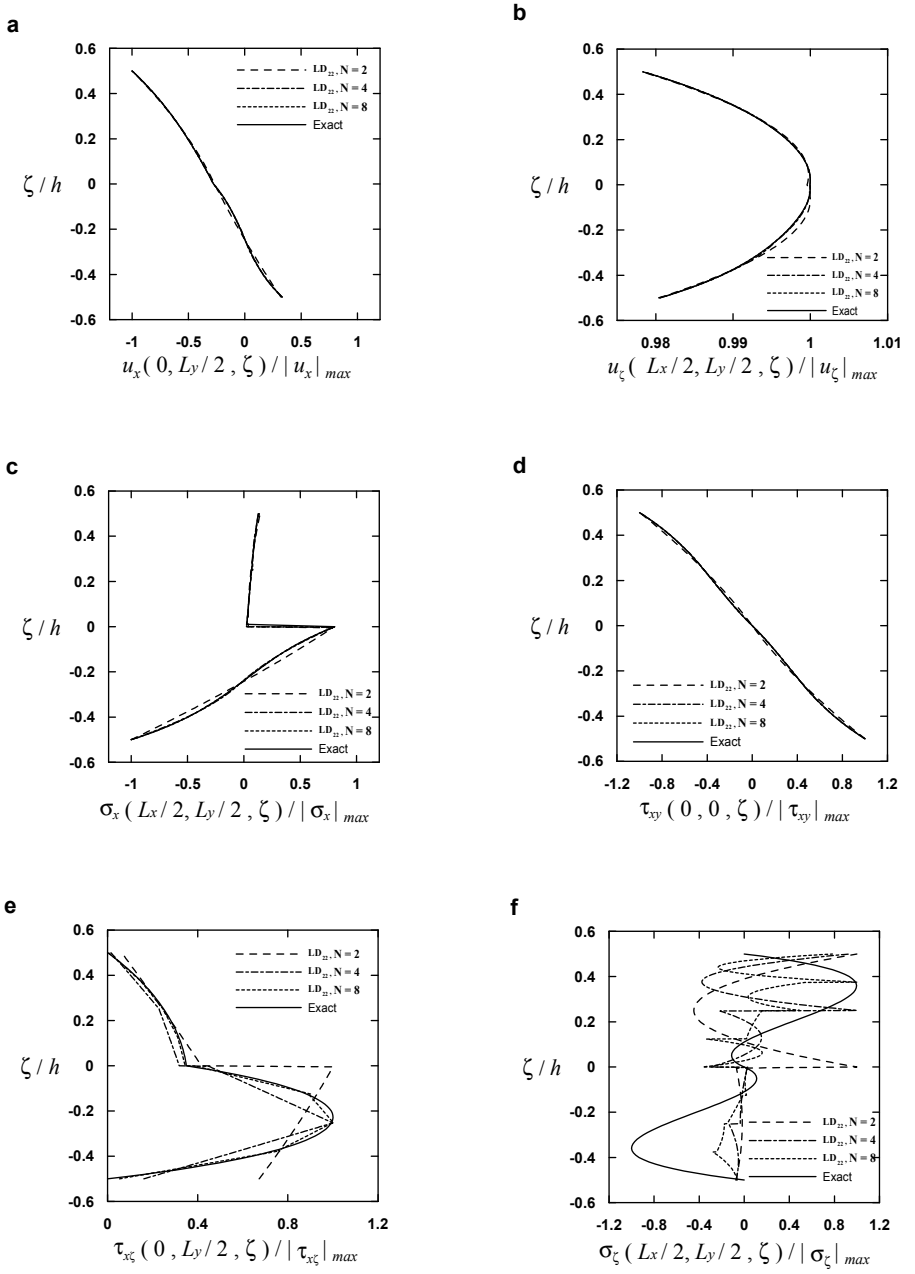

Figure 3: The through-thickness distributions of various field variables in a $[0^0/90^0]$ laminate obtained using the present LD_{22} with N=2, 4, 8 (Dynamic version of Demasi's test case 1).

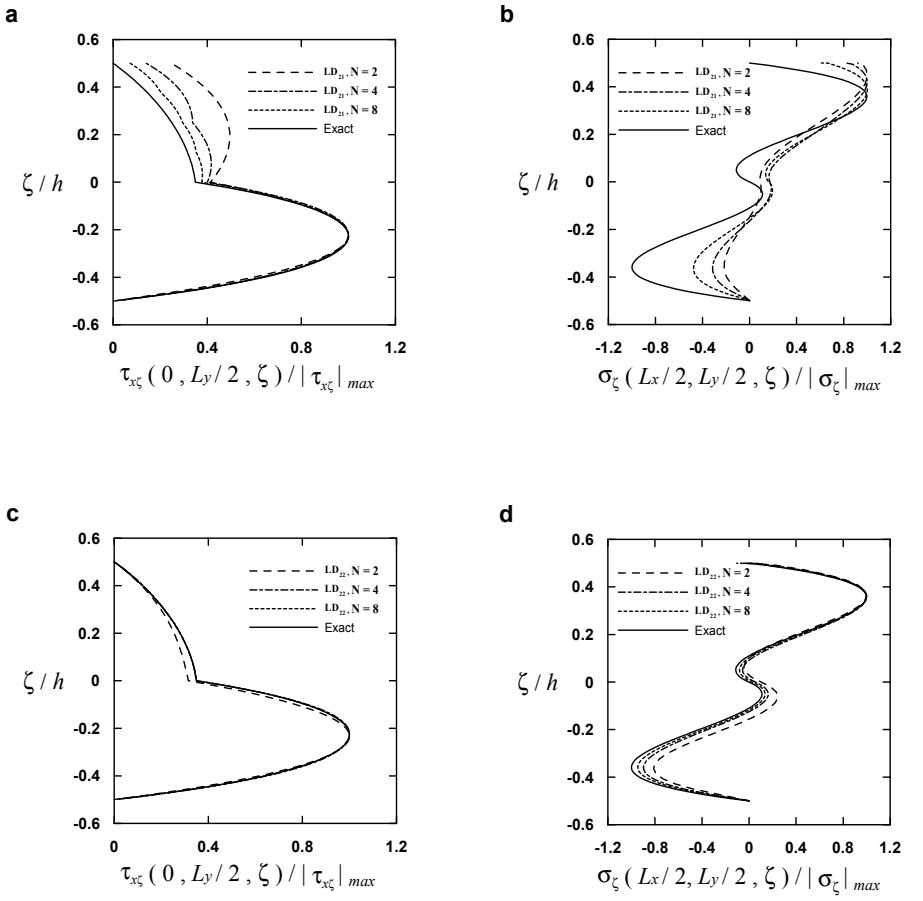

Figure 4: The through-thickness distributions of modal transverse stresses in a $[0^0/90^0]$ laminate obtained using the present LD_{21} and LD_{22} with N=2, 4, 8, where an integration approach is used (Dynamic version of Demasi's test case 1).

Dynamic-version of Pagano's benchmark case

In this case, the free vibration of the simply supported, cross-ply laminated composite elastic plates (i.e., $[0^0/90^0]$ and $[0^0/90^0/90^0/0^0]$) is studied, where the geometric parameters of the plates are taken to be $L_x/L_y = 1$, and $S = L_x/h$=2, 5, 10, 20, 50 and 100; a frequency parameter is defined as $\Omega = \left(\omega L_x^2/h\right)\sqrt{\rho/E_T}$; and the material properties are given as

$$E_L/E_T = 40, \quad G_{LT}/E_T = 0.6, \quad G_{TT}/E_T = 0.5,$$

$$E_T = 1.0\text{x}10^6\,\text{psi (or } 6.89\,\text{GPa)}, \quad \upsilon_{LT} = \upsilon_{TT} = 0.25, \tag{41}$$

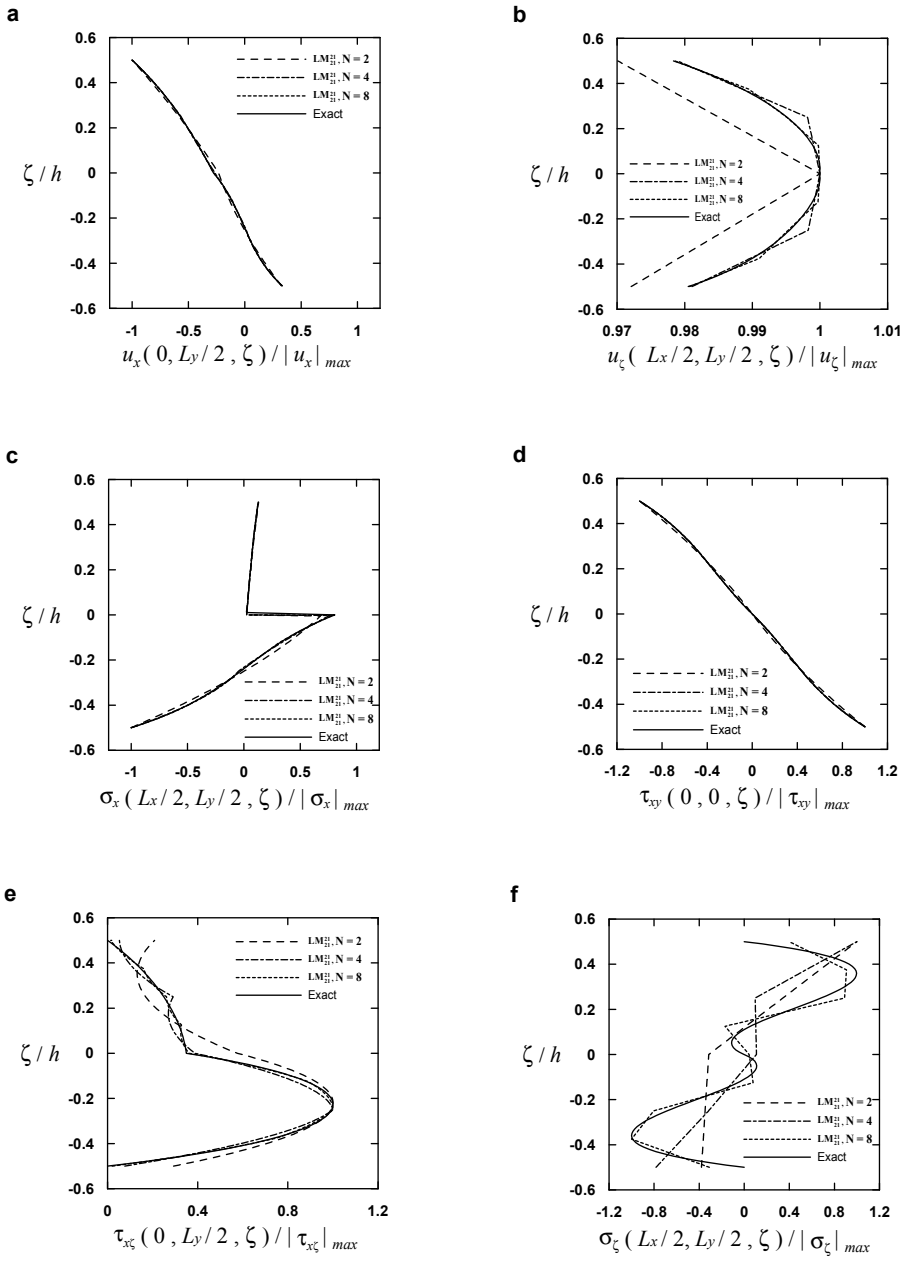

Figure 5: The through-thickness distributions of various field variables in a $\left[0^0/90^0\right]$ laminate obtained using the present LM_{21}^{21} with N=2, 4, 8 (Dynamic version of Demasi's test case 1).

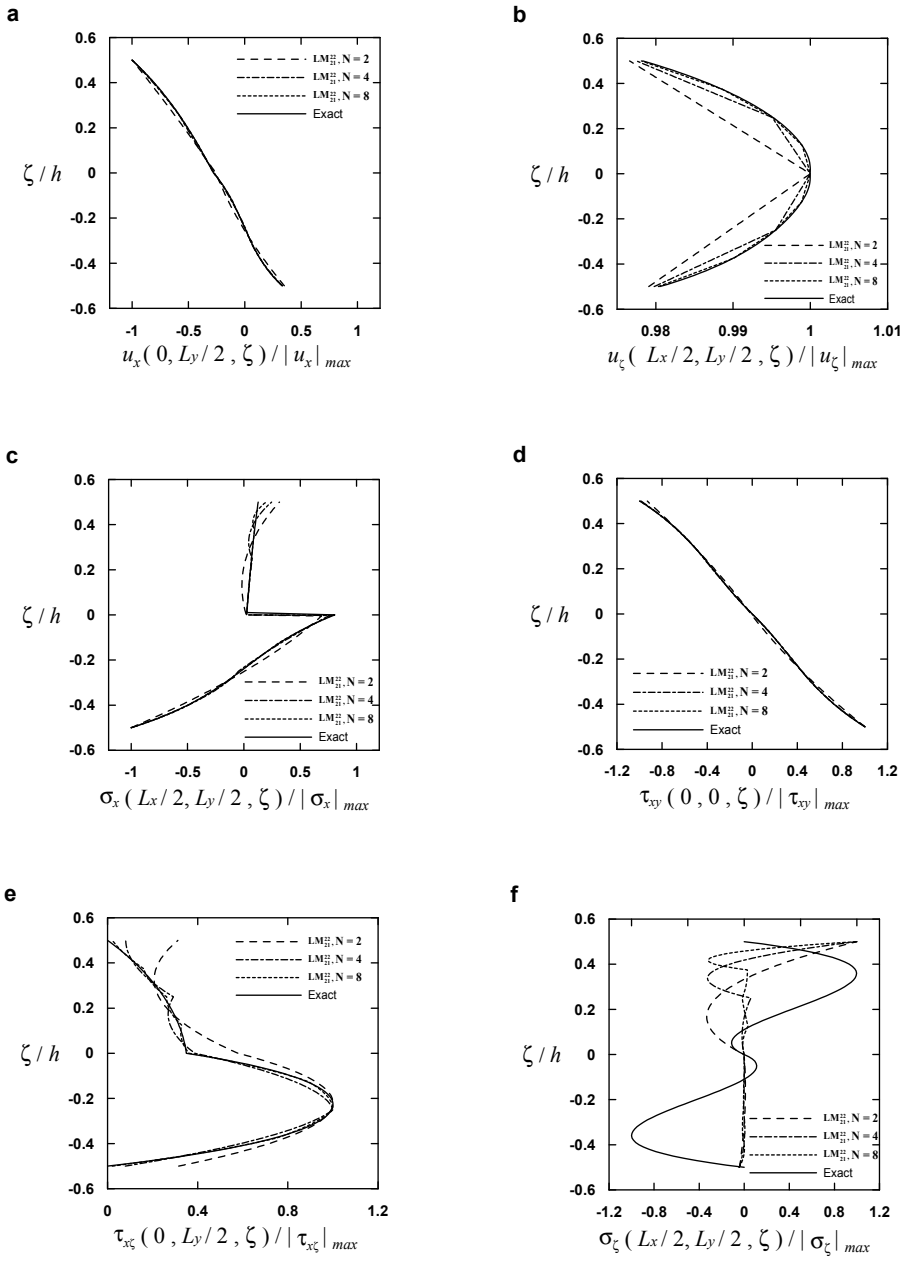

Figure 6: The through-thickness distributions of various field variables in a $[0^0/90^0]$ laminate obtained using the present LM_{21}^{22} with N=2, 4, 8 (Dynamic version of Demasi's test case 1).

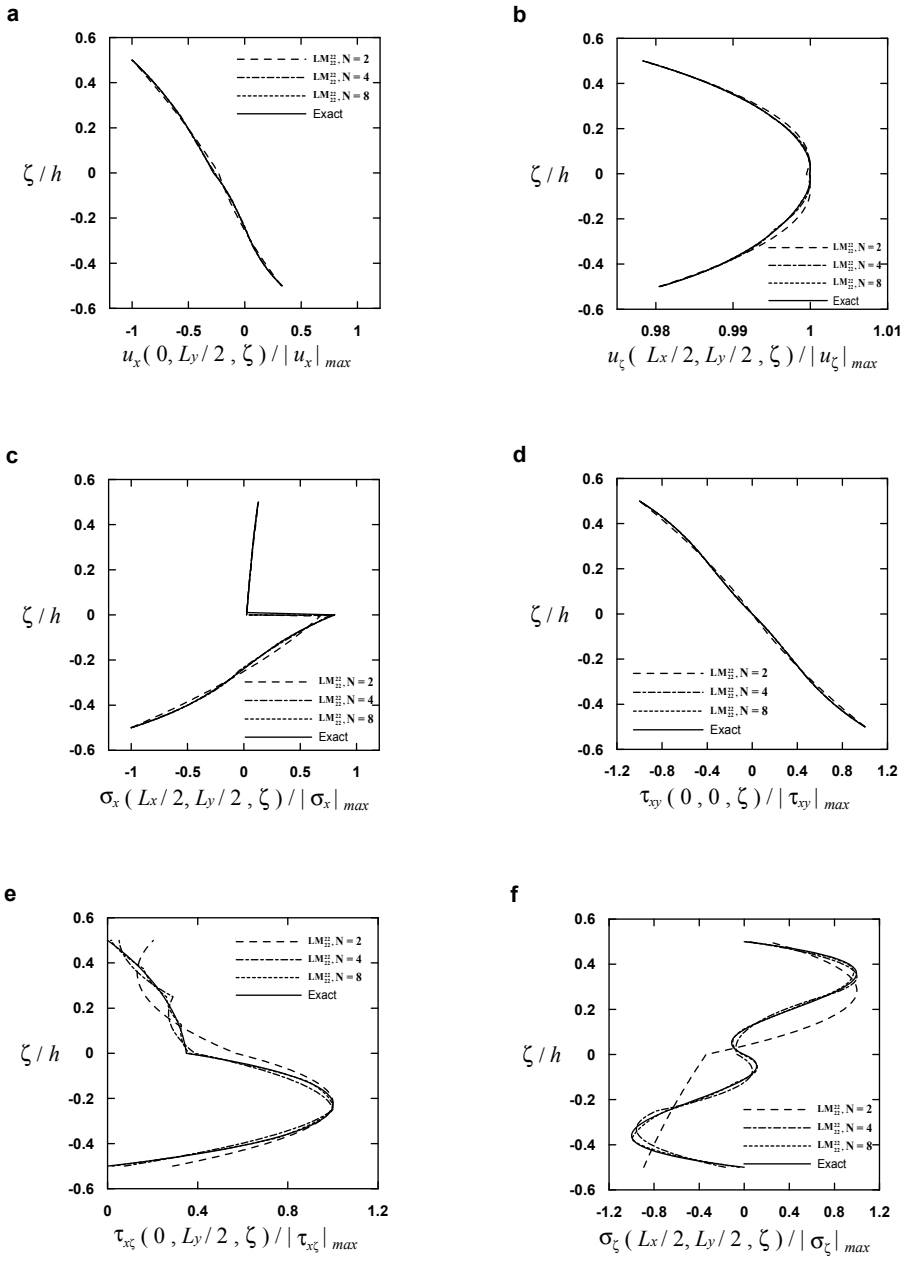

Figure 7: The through-thickness distributions of various field variables in a $\left[0^0/90^0\right]$ laminate obtained using the present LM_{22}^{22} with N=2, 4, 8 (Dynamic version of Demasi's test case 1).

where the subscripts of L and T denote the directions parallel and transverse to the fiber directions, respectively.

Table 1: Fundamental frequency parameters of laminated $\left[0^0/90^0\right]$ square plates (Dynamic-version of Demasi's test case 1)

Theories	$S = L_x/h$					
	2	5	10	20	50	100
LD_{11}(N=2)	4.567	7.865	9.405	9.980	10.165	10.192
LD_{11}(N=4)	4.481	7.635	9.082	9.620	9.791	9.817
LD_{11}(N=8)	4.373	7.495	8.965	9.517	9.694	9.720
LD_{21}(N=2)	4.526	7.819	9.381	9.973	10.163	10.192
LD_{21}(N=4)	4.369	7.523	9.033	9.605	9.789	9.816
LD_{21}(N=8)	4.333	7.460	8.950	9.512	9.693	9.720
LD_{22}(N=2)	4.444	7.550	8.969	9.495	9.663	9.688
LD_{22}(N=4)	4.337	7.448	8.926	9.482	9.661	9.688
LD_{22}(N=8)	4.323	7.440	8.923	9.482	9.661	9.688
LM_{11}^{11}(N=2)	4.367	7.487	8.946	9.489	9.662	9.688
LM_{11}^{11}(N=4)	4.367	7.455	8.925	9.482	9.661	9.688
LM_{11}^{11}(N=8)	4.329	7.441	8.923	9.482	9.661	9.688
LM_{21}^{21}(N=2)	4.382	7.488	8.942	9.487	9.662	9.688
LM_{21}^{21}(N=4)	4.329	7.444	8.924	9.482	9.661	9.688
LM_{21}^{21}(N=8)	4.322	7.440	8.923	9.482	9.661	9.688
LM_{21}^{22}(N=2)	4.451	7.673	9.209	9.791	9.978	10.006
LM_{21}^{22}(N=4)	4.349	7.474	8.961	9.522	9.703	9.729
LM_{21}^{22}(N=8)	4.327	7.445	8.928	9.487	9.666	9.693
LM_{22}^{22}(N=2)	4.381	7.486	8.942	9.487	9.662	9.688
LM_{22}^{22}(N=4)	4.327	7.443	8.924	9.482	9.661	9.688
LM_{22}^{22}(N=8)	4.322	7.440	8.923	9.482	9.661	9.688
3D exact	4.321	7.440	8.923	9.482	9.661	9.688

Tables 2–3 show the present solutions of fundamental frequency parameters of the plates with different values of the length-to-thickness ratio using various RMVT- and PVD-based FLMs, in which the plates are divided into a certain number of equal-thickness layers (N), such as N=2, 4 and 8 in Table 2 and N=4, 8 and 12 in Table 3, and the present solutions are compared with those obtained using the equivalent single layer theories (ESLTs), such as the classical plate theory (CPT), FSDT (Whitney and Pagano, 1970), Reddy TSDT (Reddy and Phan, 1985); the discrete layer theories, such as the discrete layer TSDT (Cho et al., 1991), local TSDT (Wu and Chen, 1994) and generalized TSDT (Kant and Swaminathan, 2001); and

Table 2: Fundamental frequency parameters of laminated $\left[0^0/90^0\right]$ square plates (Dynamic-version of Pagano's benchmark case)

Theories	$S = L_x/h$					
	2	5	10	20	50	100
LD_{11}(N=2)	5.119	8.734	10.453	11.094	11.299	11.329
LD_{11}(N=4)	5.086	8.700	10.424	11.069	11.275	11.306
LD_{11}(N=8)	4.997	8.578	10.362	11.046	11.267	11.299
LD_{21}(N=2)	5.083	8.708	10.441	11.090	11.298	11.329
LD_{21}(N=4)	4.974	8.544	10.348	11.046	11.271	11.305
LD_{21}(N=8)	4.956	8.529	10.338	11.039	11.265	11.299
LD_{22}(N=2)	5.073	8.689	10.414	11.061	11.268	11.298
LD_{22}(N=4)	4.970	8.539	10.341	11.038	11.264	11.297
LD_{22}(N=8)	4.955	8.528	10.337	11.037	11.264	11.297
LM_{11}^{11}(N=2)	5.007	8.579	10.362	11.045	11.265	11.298
LM_{11}^{11}(N=4)	5.017	8.572	10.353	11.041	11.264	11.297
LM_{11}^{11}(N=8)	4.965	8.531	10.338	11.037	11.264	11.297
LM_{21}^{21}(N=2)	5.030	8.614	10.377	11.049	11.266	11.298
LM_{21}^{21}(N=4)	4.964	8.534	10.339	11.038	11.264	11.297
LM_{21}^{21}(N=8)	4.954	8.527	10.337	11.037	11.264	11.297
LM_{21}^{22}(N=2)	5.035	8.625	10.393	11.068	11.285	11.317
LM_{21}^{22}(N=4)	4.965	8.535	10.341	11.040	11.266	11.300
LM_{21}^{22}(N=8)	4.955	8.528	10.337	11.037	11.264	11.298
LM_{22}^{22}(N=2)	5.027	8.611	10.377	11.049	11.266	11.298
LM_{22}^{22}(N=4)	4.961	8.533	10.339	11.038	11.264	11.297
LM_{22}^{22}(N=8)	4.954	8.527	10.337	11.037	11.264	11.297
CPT	8.499	10.584	11.011	11.125	11.158	11.163
FSDT	5.191	8.757	10.355	10.941	11.127	11.155
Reddy TSDT	5.699	9.010	10.449	10.968	11.132	11.156
Generalized TSDT	5.074	NA	10.415	11.051	11.253	11.283
Discrete layer TSDT	4.810	8.388	10.270	11.016	11.260	11.296
Local TSDT	4.959	8.527	10.337	11.037	11.264	11.297
3D FE model	4.953	8.527	10.338	11.040	11.267	11.298
3D exact	4.953	8.527	10.336	11.037	11.264	11.297

Table 3: Fundamental frequency parameters of laminated $\left[0^0/90^0/90^0/0^0\right]$ square plates (Dynamic-version of Pagano's benchmark cases)

Theories	$S = L_x/h$					
	2	5	10	20	50	100
LD_{11}(N=4)	5.458	10.891	15.219	17.700	18.686	18.843
LD_{11}(N=8)	5.367	10.741	15.108	17.652	18.674	18.837
LD_{11}(N=12)	5.340	10.709	15.086	17.643	18.672	18.836
LD_{21}(N=4)	5.345	10.696	15.076	17.641	18.675	18.840
LD_{21}(N=8)	5.319	10.684	15.070	17.637	18.671	18.836
LD_{21}(N=12)	5.316	10.683	15.069	17.636	18.670	18.836
LD_{22}(N=4)	5.338	10.691	15.072	17.636	18.670	18.835
LD_{22}(N=8)	5.317	10.683	15.069	17.636	18.670	18.835
LD_{22}(N=12)	5.315	10.682	15.069	17.636	18.670	18.835
LM_{11}^{11}(N=4)	5.357	10.766	15.136	17.664	18.675	18.837
LM_{11}^{11}(N=8)	5.329	10.687	15.070	17.636	18.670	18.835
LM_{11}^{11}(N=12)	5.318	10.684	15.070	17.636	18.670	18.835
LM_{21}^{21}(N=4)	5.325	10.687	15.070	17.636	18.670	18.835
LM_{21}^{21}(N=8)	5.316	10.683	15.069	17.636	18.670	18.835
LM_{21}^{21}(N=12)	5.315	10.682	15.069	17.636	18.670	18.835
LM_{21}^{22}(N=4)	5.334	10.690	15.072	17.638	18.672	18.837
LM_{21}^{22}(N=8)	5.317	10.683	15.069	17.636	18.670	18.835
LM_{21}^{22}(N=12)	5.315	10.682	15.069	17.636	18.670	18.835
LM_{22}^{22}(N=4)	5.326	10.687	15.070	17.636	18.670	18.835
LM_{22}^{22}(N=8)	5.316	10.682	15.069	17.636	18.670	18.835
LM_{22}^{22}(N=12)	5.315	10.682	15.069	17.636	18.670	18.835
CPT	15.830	18.215	18.652	18.767	18.799	18.804
FSDT	5.492	10.820	15.083	17.583	18.590	18.751
Reddy TSDT	5.576	10.989	15.270	17.668	17.606	18.755
Generalized TSDT	5.393	NA	15.095	17.643	18.671	18.835
Discrete layer TSDT	5.923	10.673	15.066	17.535	18.670	18.835
3D FE model	5.315	10.682	15.069	17.636	18.670	18.835
3D exact	5.315	10.682	15.069	17.636	18.670	18.835

Table 4: The least frequency parameters of the flexural and extensional modes of single-layer functionally graded elastic plates

$S\ (L_x/h)$	κ_p	Modes	Present theories						3D asymptotic theory	Discrete layer theory	3D exact theory
			LD_{22}			LM_{22}^{22}					
			$N_L=4$	$N_L=8$	$N_L=12$	$N_L=4$	$N_L=8$	$N_L=12$			
5	1	Flexural mode	5.5476	5.5473	5.5473	5.5466	5.5464	5.5464	5.5473	5.478	5.480
		Extensional mode	14.8605	14.8605	14.8605	14.8605	14.8605	14.8605	14.8605	14.550	14.733
		Extensional mode	24.7712	24.7712	24.7712	24.7449	24.7449	24.7449	24.7718	24.365	24.380
5	2	Flexural mode	5.5425	5.5422	5.5422	5.5412	5.5410	5.5410	5.5422	5.490	5.493
		Extensional mode	14.5396	14.5396	14.5396	14.5396	14.5396	14.5396	14.5396	14.270	14.278
		Extensional mode	24.2462	24.2461	24.2461	24.2133	24.2132	24.2132	24.2469	23.898	23.910
5	3	Flexural mode	5.5729	5.5726	5.5725	5.5713	5.5712	5.5712	5.5726	5.528	5.528
		Extensional mode	14.3717	14.3717	14.3717	14.3717	14.3717	14.3717	14.3717	14.145	14.150
		Extensional mode	23.9797	23.9796	23.9796	23.9412	23.9411	23.9411	23.9805	23.688	23.695
5	5	Flexural mode	5.6040	5.6036	5.6036	5.6022	5.6021	5.6021	5.6036	5.563	5.563
		Extensional mode	14.1928	14.1928	14.1928	14.1928	14.1928	14.1928	14.1928	14.023	14.025
		Extensional mode	23.7046	23.7043	23.7043	23.6604	23.6603	23.6603	23.7052	23.488	23.495
10	1	Flexural mode	6.0228	6.0227	6.0227	6.0227	6.0227	6.0227	6.0227	5.960	5.960
		Extensional mode	29.7275	29.7275	29.7275	29.7275	29.7275	29.7275	29.7275	29.100	29.120
		Extensional mode	49.7694	49.7694	49.7694	49.7668	49.7667	49.7667	49.7694	48.980	49.010
20	1	Flexural mode	6.1674	6.1674	6.1674	6.1674	6.1674	6.1674	6.1674	6.120	6.120
		Extensional mode	59.4583	59.4583	59.4583	59.4583	59.4583	59.4583	59.4583	58.200	58.240
		Extensional mode	99.6456	99.6455	99.6455	99.6452	99.6452	99.6452	99.6457	98.080	98.160

Table 5: The least requency parameters of two-layered functionally graded elastic plates for some fixed mode shapes

$S\ (L_x/h)$	κ_e	$(\hat{m},\ \hat{n})$	Present theories						3D exact theory
			LD_{22}			LM_{22}^{22}			
			$N_L=4$	$N_L=8$	$N_L=12$	$N_L=4$	$N_L=8$	$N_L=12$	
5	1	(1 , 1)	1.7636	1.7634	1.7633	1.7635	1.7634	1.7633	1.7633
		(1 , 2)	2.4337	2.4334	2.4333	2.4335	2.4333	2.4333	2.4333
		(2, 2)	4.1945	4.1891	4.1887	4.1927	4.1889	4.1887	4.1886
5	2	(1 , 1)	1.6609	1.6604	1.6604	1.6608	1.6604	1.6604	1.6604
		(1 , 2)	2.2964	2.2955	2.2955	2.2961	2.2955	2.2955	2.2955
		(2, 2)	3.9436	3.9377	3.9373	3.9415	3.9375	3.9372	3.9372
5	3	(1 , 1)	1.5004	1.4984	1.4982	1.5001	1.4983	1.4982	1.4982
		(1 , 2)	2.0676	2.0644	2.0642	2.0670	2.0643	2.0642	2.0641
		(2, 2)	3.6166	3.6094	3.6088	3.6144	3.6092	3.6088	3.6087
5	5	(1 , 1)	1.1177	1.1090	1.1085	1.1161	1.1090	1.1084	1.1083
		(1 , 2)	1.5189	1.5061	1.5053	1.5165	1.5060	1.5053	1.5050
		(2, 2)	2.9260	2.9150	2.9141	2.9224	2.9147	2.9141	2.9139
10	1	(1 , 1)	2.5842	2.5842	2.5842	2.5842	2.5842	2.5842	2.5841
		(1 , 2)	3.5011	3.5011	3.5011	3.5011	3.5011	3.5011	3.5011
		(2, 2)	7.0545	7.0534	7.0534	7.0541	7.0534	7.0534	7.0533
20	1	(1 , 1)	3.1193	3.1193	3.1193	3.1193	3.1193	3.1193	3.1193
		(1 , 2)	4.1849	4.1849	4.1849	4.1849	4.1849	4.1849	4.1849
		(2, 2)	10.3367	10.3366	10.3366	10.3367	10.3366	10.3366	10.3366

the 3D theories, such as the 3D FEM (Desai et al., 2003) and 3D modified Pagano theories (Wu and Lü, 2009). By comparing the present solutions of various RMVT- and PVD-based FLMs with the 3D exact solutions obtained using the modified Pagano method (Wu and Lü, 2009), we obtain the same conclusions as those in the dynamic-version of Demasi's test case 1, which are $\mathrm{LD}_{22} > \mathrm{LD}_{21} > \mathrm{LD}_{11}$, $\mathrm{LM}_{22}^{22} > \mathrm{LM}_{21}^{21} > \mathrm{LM}_{21}^{22} > \mathrm{LM}_{11}^{11}$. The present convergent solutions of LD_{22}, LM_{21}^{21} and LM_{22}^{22} are in excellent agreement with the 3D exact solutions, and are superior to those obtained with the other 2D TSDT theories mentioned above.

4.2 Single-layer FGM plates

In this case, the free vibration of a simply-supported, single-layer square plate composed of FG isotropic elastic material is investigated, and this problem has also been studied by Ramirez (2006b), Vel and Batra (2004) and Wu and Tsai (2010) using a discrete layer, power series expansion and multiple scale methods, respectively. The plate considered is made of aluminum (Al) and zirconia (ZrO_2), the material properties of which are given as follows:

For Al,

$$c_{11} = c_{22} = c_{33} = 94.231 \text{ GPa}, \quad c_{12} = c_{13} = c_{23} = 40.385 \text{ GPa},$$
$$c_{44} = c_{55} = c_{66} = 26.923 \text{ GPa}, \quad \rho = 2702 \text{ Kg / m}^3; \tag{42}$$

For ZrO_2,

$$c_{11} = c_{22} = c_{33} = 269.23 \text{ GPa}, \quad c_{12} = c_{13} = c_{23} = 115.38 \text{ GPa},$$
$$c_{44} = c_{55} = c_{66} = 76.923 \text{ GPa}, \quad \rho = 5700 \text{ Kg / m}^3. \tag{43}$$

The volume fractions of the ceramic phase (V_c) and of the metal phase (V_m) are assumed to vary through the thickness coordinate in the following forms:

$$V_c(\zeta) = \left[\frac{\zeta + (h/2)}{h}\right]^{\kappa_p} \text{ and } V_m(\zeta) = 1 - V_c(\zeta), \tag{44}$$

where κ_p is the material-property gradient index.

The material properties of the FG elastic plate depend upon the volume fractions V_c and V_m, and are determined using the Mori-Tanaka scheme, which was also adopted in Ramirez et al. (2006a) , Vel and Batra (2004) and Wu and Tsai (2010). The effective material properties of this are expressed as follows:

$$\rho(\zeta) = \rho_c V_c(\zeta) + \rho_m V_m(\zeta), \tag{45a}$$

$$K(\zeta) = \frac{V_c(\zeta)(K_c - K_m)}{\left[1 + (1 - V_c(\zeta))\frac{K_c - K_m}{K_m + (4/3)\mu_m}\right]} + K_m, \tag{45b}$$

$$\mu(\zeta) = \frac{V_c(\zeta)(\mu_c - \mu_m)}{\left[1 + (1 - V_c(\zeta))\frac{\mu_c - \mu_m}{\mu_c + f_m}\right]} + \mu_m, \tag{45c}$$

$$f_m = \mu_m \frac{9K_m + 8\mu_m}{6(K_m + 2\mu_m)}, \tag{45d}$$

$$\lambda(\zeta) = K(\zeta) - 2\mu(\zeta)/3, \tag{45e}$$

where $K(\zeta)$, K_c and K_m are the bulk moduli of the composite, ceramic and metal materials, respectively; $\mu(\zeta)$, μ_c and μ_m are the shear moduli; $\lambda(\zeta)$, λ_c and λ_m are the Lame constants.

The through-thickness engineering elastic constants of the plate can then be determined by

$$c_{11}(\zeta) = c_{22}(\zeta) = c_{33}(\zeta) = \lambda(\zeta) + 2\mu(\zeta), \tag{46a}$$

$$c_{44}(\zeta) = c_{55}(\zeta) = c_{66}(\zeta) = \mu(\zeta), \tag{46b}$$

$$c_{23}(\zeta) = c_{13}(\zeta) = c_{12}(\zeta) = \lambda(\zeta). \tag{46c}$$

The geometric parameters are taken as $L_x/L_y = 1$; $L_x/h = 5,\ 10,\ 20$; the material property gradient index is taken as $\kappa_p = 1,\ 2,\ 3,\ 5$; and a frequency parameter Ω is defined as $\Omega = \omega L_x^2 \sqrt{\rho^{(b)}/E_{11}^{(b)}}/h$, where the superscript b in the parenthesis denotes the bottom surface of the plate and $E_{11}^{(b)}$=70 GPa in the case.

The LD_{22} and LM_{22}^{22} solutions of the least frequency parameters of the flexural and extensional modes of these metal-ceramic composite graded plates are presented in Table 4, where the wave numbers of $\hat{m}$ and $\hat{n}$ are fixed at $\hat{m}$=1 and $\hat{n}$=1. It is shown that the rate of convergence of the present solutions is rapid. As κ_p=1, the convergent solutions of the least frequency parameter of the flexural mode are yielded at N=4 for thin plates ($L_x/h = 20$), N=8 for thick plates ($L_x/h = 5$), and those of extensional modes are yielded at N=4 for both thin and thick plates. The present eight-layer solutions of LD_{22} and LM_{22}^{22} are in good agreement with the discrete layer (Ramirez et al., 2006b), 3D exact (Vel and Batra , 2004) and 3D asymptotic (Wu and Tsai, 2010) solutions. Fig. 8 shows the variations of the through-thickness distributions of modal displacements and stresses with κ_p, in which N=12, S=5 and κ_p=1, 2, 5.

It is seen in Fig. 8 that the effect of κ_p on the through-thickness distribution of modal displacement and stress components is minor, and the through-thickness distribution of modal in-plane displacement appears to be linear, and those of out-of-plane displacement and stresses are higher-degree polynomial functions.

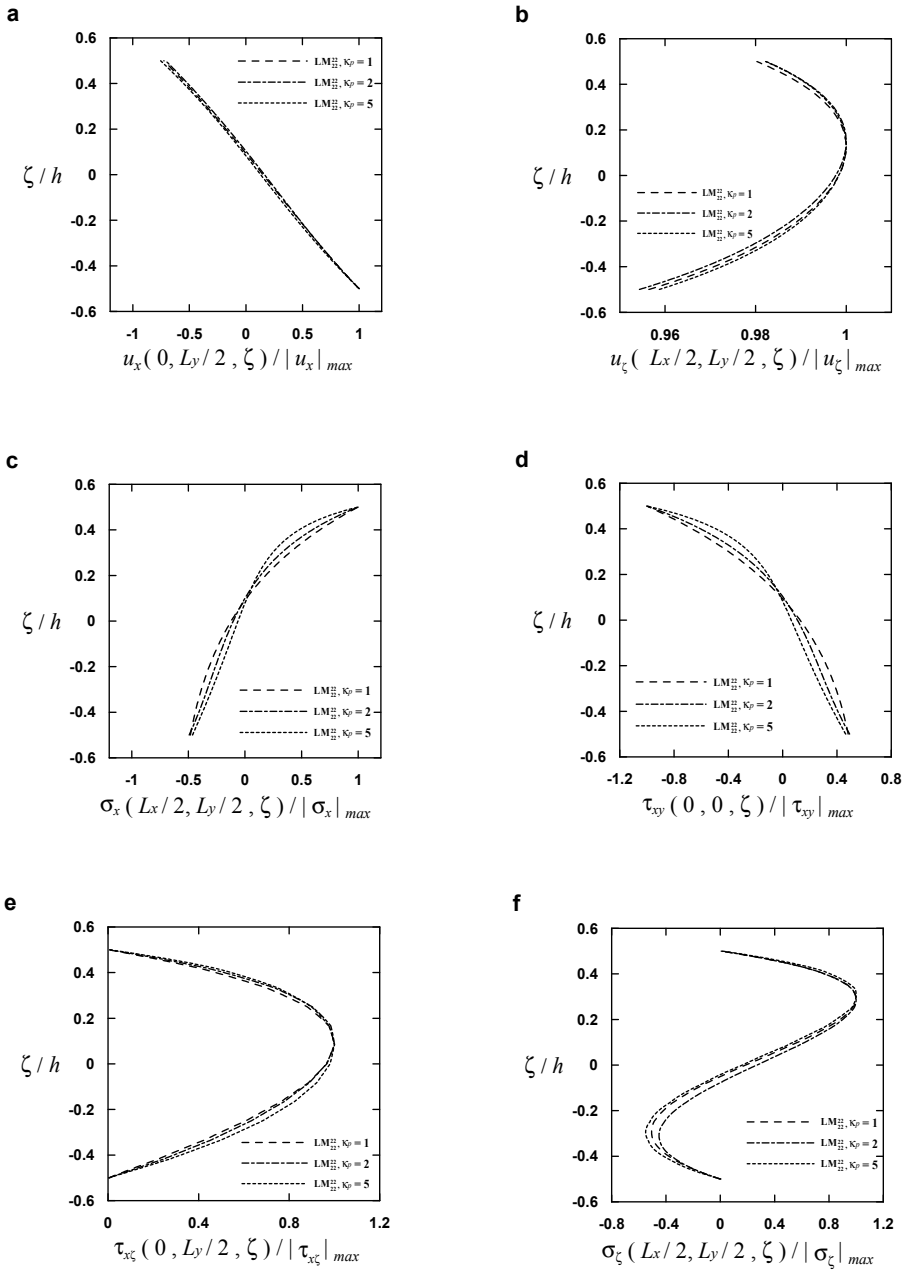

Figure 8: Variations of the 12-layer LM_{22}^{22} solutions of the through-thickness distributions of various modal field variables in a single-layer FGM plate with κ_p.

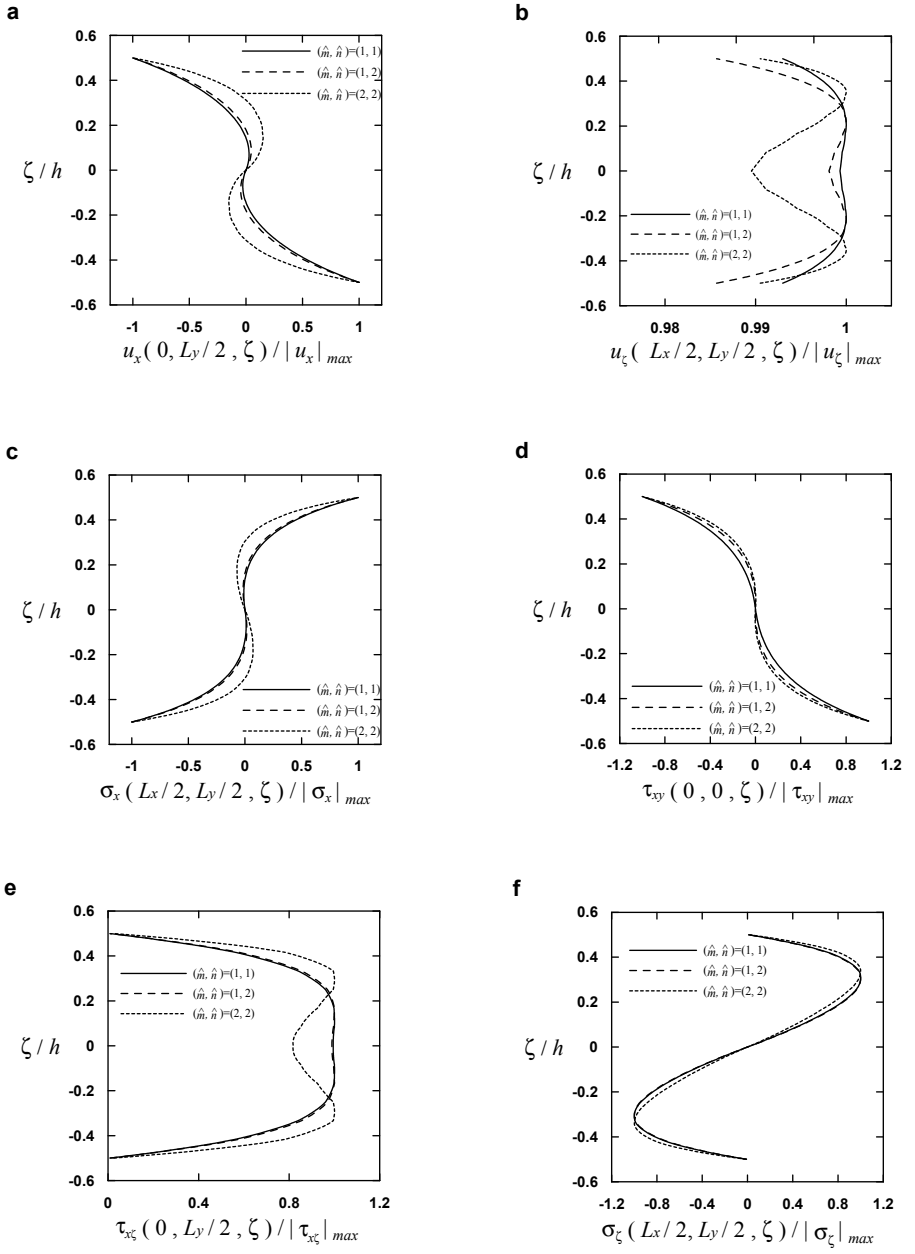

Figure 9: Variations of the 12-layer LM_{22}^{22} solutions of the through-thickness distributions of various modal field variables in a two-layered FGM plate with wave numbers $(\hat{m},\ \hat{n})$.

4.3 Multilayered FGM plates

In this case, the free vibration of simply-supported, two-layered square plates composed of FGM orthotropic layers (i.e., [FGM/FGM] plates) is studied. The material properties of each layer are assumed to obey an exponent-law exponentially varied with the thickness coordinate of the plate, and given as

$$c_{ij} = c_{ij}^{(0)} e^{\kappa_e [\zeta/(h/2)]} \text{ when } 0 \le \zeta \le h/2, \tag{47a}$$

$$c_{ij} = c_{ij}^{(0)} e^{\kappa_e [\zeta/(-h/2)]} \text{ when } -h/2 \le \zeta \le 0, \tag{47b}$$

where κ_e denotes the material-property gradient index, and is taken as $\kappa_e = 1,\ 2,\ 3$ and 5; when $\kappa_e = 0$, the plates reduce to single-layer orthotropic plates (i.e., $\left[0^0\right]$ plates); and $c_{ij}^{(0)}$ represents the material properties of the reference material (i.e., those of 0^0 layer), and is given as follows:

$$c_{11}^{(0)} = 2.51678 \times 10^6 \text{ psi (or } 173.40604 \text{ GPa)},$$

$$c_{12}^{(0)} = c_{13}^{(0)} = 2.51678 \times 10^6 \text{ psi (or } 2.31208 \text{ GPa)},$$

$$c_{22}^{(0)} = c_{33}^{(0)} = 1.07114 \times 10^6 \text{ psi (or } 7.38016 \text{ GPa)},$$

$$c_{23}^{(0)} = 0.27114 \times 10^6 \text{ psi (or } 1.86816 \text{ GPa)},$$

$$c_{44}^{(0)} = 0.2 \times 10^6 \text{ psi (or } 1.378 \text{ GPa)},$$

$$c_{55}^{(0)} = c_{66}^{(0)} = 0.5 \times 10^6 \text{ psi (or } 3.445 \text{ GPa)},$$

$$\rho^{(0)} = 1590 \text{ Kg / m}^3,$$

which are transformed from the engineering constants of the 0^0 layer, which are given in Eq. (41).

Table 5 presents the least frequency parameters of the [FGM/FGM] square plates for some fixed mode shapes, in which $\kappa_e = 1,\ 2,\ 3$ and 5, S=5, 10 and 20, and $(\hat{m},\ \hat{n}) = (1,\ 1),\ (1,\ 2)$ and $(2,\ 2)$. Again, it is shown that the convergence of the solutions of LD_{22} and LM_{22}^{22} are yielded at N=8, and the convergent solutions are in excellent agreement with the 3D exact solutions obtained using the modified Pagano method (Wu and Lü, 2009). Fig. 9 shows that the variation of the through-thickness distribution of modal field variables with wave numbers, in which S=5, $\kappa_e = 1$, N=12, and $(\hat{m},\ \hat{n}) = (1,\ 1)$, (1, 2) and (2, 2). It is seen in Fig. 9 that the through-thickness distributions of modal field variables in the case of $(\hat{m},\ \hat{n}) = (1,\ 1)$, which is the fundamental mode, are not much different from those in the case of $(\hat{m},\ \hat{n}) = (1,\ 2)$, while much differ from those in the case of $(\hat{m},\ \hat{n}) = (2,\ 2)$.

5 Concluding remarks

In this work, we developed the unified formulations of various RMVT- and PVD-based FLMs to investigate the free vibration of simply supported, multilayered composite and FGM plates. The dynamic-versions of Demasi's test and Pagano's benchmark cases were used to validate the accuracy and convergence rate of these RMVT- and PVD-based FLMs, and the so-called numerical instability problems resulting from the relative orders used for expansion to the displacement and stress components in the RMVT-based theories were also examined. In the implementation of various RMVT- and PVD-based FLMs with the *h*-refinement process, we found that $\mathrm{LD}_{22} > \mathrm{LD}_{21} > \mathrm{LD}_{11}$ and $\mathrm{LM}_{22}^{22} > \mathrm{LM}_{21}^{21} > \mathrm{LM}_{21}^{22} > \mathrm{LM}_{11}^{11}$, which means LD_{22} is superior to other PVD-based FLMs, and LM_{22}^{22} is superior to other RMVT-based FLMs. By observing the through-thickness distributions of modal displacement and stress components obtained using various FLMs, we found both LD_{22} and LM_{22}^{22} may lead to satisfactory results in comparison with the available 3D exact solutions, where the modal transverse stresses were determined using an integration approach in LD_{22} and using the interpolation functions a priori in LM_{22}^{22}. In addition, although the LM_{21}^{22} theory may lead to accurate results for the natural frequency parameters of the laminated composite and FGM plates, the through-thickness distributions of the modal transverse normal stress obtained using the interpolation functions a priori in LM_{21}^{22} oscillate in the top layer, and the LM_{21}^{22} theory fails to yield the satisfactory predictions for these. This observation coincides with Demasi's conclusion, which is that numerical instability occurs when the relative orders used for expansion to the out-of-plane displacement and transverse normal stress are different to each other. Moreover, the overall performance of the RMVT-based FLMs is superior to that of the PVD-based FLMs.

Acknowledgement: This work was supported by the National Science Council of Republic of China through Grant NSC 97-2221-E006-128-MY3.

References

Akhras, G.; Li, W.C. (2007): Three-dimensional static, vibration and stability analysis of piezoelectric composite plates using a finite layer method. *Smart Mater. Struct.*, vol. 16, pp. 561–569.

Akhras, G.; Li, W.C. (2008): Three-dimensional thermal buckling analysis of piezoelectric composite plates using the finite layer method. *Smart Mater. Struct.*, vol. 17, pp. 1–8.

Brischetto, S.; Leetsch, R.; Carrera, E.; Wallmersperger, T.; Kroplin, B. (2008): Thermo-mechanical bending of functionally graded plates. *J. Therm. Stresses*, vol.

31, pp. 286–308.

Brischetto, S.; Carrera, E. (2008): Advanced mixed theories for bending analysis of functionally graded plates. *Comput. Struct*. doi:10.1016/j.compstruc.2008.04.004.

Brischetto, S.; Carrera, E. (2009): Refined 2D models for the analysis of functionally graded piezoelectric plates. *J. Intell. Mater. Sys. Struct*., vol. 20, pp. 1783–1797.

Carrera, E. (1999): A study of transverse normal stress effect on vibration of multilayered plates and shells. *J. Sound Vib.*, vol. 225, pp. 803–829.

Carrera, E. (2000a): An assessment of mixed and classical theories on global and local response of multilayered orthotropic plates. *Compos. Struct*., vol. 50, pp. 183–198.

Carrera, E. (2000b): An assessment of mixed and classical theories for the thermal stress analysis of orthotropic multilayered plates. *J. Therm. Stresses*, vol. 23, pp. 797–831.

Carrera, E. (2001): Developments, ideas, and evaluations based upon Reissner's Mixed Variational Theorem in the modeling of multilayered plates and shells. *Appl. Mech. Rev*., vol. 54, pp. 301–329.

Carrera, E. (2003a): Historical review of zig-zag theories for multilayered plates and shells. *Appl. Mech. Rev*., vol. 56, pp. 287–308.

Carrera, E. (2003b): Theories and finite elements for multilayered plates and shells: A unified compact formulation with numerical assessment and benchmarks. *Arch. Comput. Methods Eng.*, vol. 10, pp. 215–296.

Carrera, E. (2004): Assessment of theories for free vibration analysis of homogeneous and multilayered plates. *Shock Vib*., vol. 11, pp. 261–270.

Carrera, E.; Brischetto, S.; Robaldo, A. (2008): Variable kinematic model for the analysis of functionally graded material plates. *AIAA J*., vol. 46, pp. 194–203.

Carrera, E.; Giunta, G.; Brischetto, S. (2007): Hierarchical closed form solutions for plates bent by localized transverse loadings. *J. Zhejiang Univ.: Science A*, vol. 8, pp. 1026–1037.

Cheung, Y.K. (1976): Finite Strip Method in Structural Analysis. Pergamon Press, Oxford, UK.

Cheung, Y.K.; Jiang, C.P. (2001): Finite layer method in analysis of piezoelectric composite laminates. *Comput. Methods Appl. Mech. Eng*., vol. 191, pp. 879–901.

Cho, K.N.; Bert, C.W.; Striz, A.G. (1991): Free vibrations of laminated rectangular plates analyzed by higher order individual-layer theory. *J. Sound Vib*., vol. 145, pp. 429–442.

Demasi, L. (2008a): ∞^3 hierarchy plate theories for thick and thin composite plates: The Generalized Unified Formulation. *Compos. Struct.*, vol. 84, pp. 256–270.

Demasi, L. (2008b): 2D, quasi 3D and 3D exact solutions for bending of thick and thin sandwich plates. *J. Sandw. Struct. Mater* ., vol. 10, pp. 271–310.

Demasi, L. (2009a): ∞^6 mixed plate theories based on the Generalized Unified Formulation, Part I: Governing equations. *Compos. Struct.*, vol. 87, pp. 1–11.

Demasi, L. (2009b): ∞^6 mixed plate theories based on the Generalized Unified Formulation, Part II: Layerwise theories. *Compos. Struct.*, vol. 87, pp. 12–22.

Demasi, L. (2009c): ∞^6 mixed plate theories based on the Generalized Unified Formulation, Part III: Advanced mixed high order shear deformation theories. *Compos. Struct.*, vol. 87, pp. 183–194.

Demasi, L. (2009d): ∞^6 mixed plate theories based on the Generalized Unified Formulation, Part IV: Zig-zag theories. *Compos. Struct.*, vol. 87, pp. 195–205.

Demasi, L. (2009e): ∞^6 mixed plate theories based on the Generalized Unified Formulation, Part V: Results. *Compos. Struct.*, vol. 88, pp. 1–16.

Desai, Y.M.; Ramtekkar, G.S.; Shah, A.H. (2003): Dynamic analysis of laminated composite plates using a layer-wise mixed finite element model. *Compos. Struct.*, vol. 59, pp. 237–249.

Heyliger, P. (1997): Exact solutions for simply supported laminated piezoelectric plates. *J. Appl. Mech.*, vol. 63, pp. 299–306.

Hill, R. (1965): A self-consistent mechanics of composite materials. *J. Mech. Phy. Solids*, vol. 13, pp. **213–222.**

Hussein, M.; Heyliger, P.R. (1996): Discrete layer analysis of axisymmetric vibrations of laminated piezoelectric cylinders. *J. Sound Vib.*, vol. 192, pp. 995–1013.

Kant, T.; Pendhari, S.S.; Desai, Y.M. (2007): A general partial discretization methodology for interlaminar stress computation in composite laminates. *CMES: Comput. Modeling Eng. Sci.*, vol. 17, pp. 135–161.

Kant, T.; Swaminathan, K. (2001): Analytical solutions for free vibration of laminated composite and sandwich plates based on a higher-order refined theory. *Compos. Struct.*, vol. 53, pp. 73–85.

Kardomateas, G.A. (2009): Three-dimensional elasticity solution for sandwich plates with orthotropic phases: The positive discriminant case. *J. Appl. Mech.*, vol. 76, pp. 1–4.

Kashtalyan, M. (2004): Three-dimensional elasticity solution for bending of functionally graded rectangular plates. *Eur. J. Mech. A/Solids*, vol. 23, pp. 853–864.

Li, Q.; Iu, V.P.; Kou, K.P. (2008): Three-dimensional vibration analysis of func-

tionally graded material sandwich plates. *J. Sound Vib.*, vol. 311, pp. 498–515.

Lü C.F.; Chen, W.Q.; Shao, J.W. (2008): Semi-analytical three-dimensional elasticity solutions for generally laminated composite plates. *Eur. J. Mech. A/Solids*, vol. 27, pp. 899–917.

Lü, C.F.; Huang, Z.Y.; Chen, W.Q. (2007): Semi-analytical solutions for free vibration of anisotropic laminated plates in cylindrical bending. *J. Sound Vib.*, vol. 304, pp. 987–995.

Mori, T.; Tanaka, K. (1973): Average stress in matrix and average elastic energy of materials with misfitting inclusions. *Acta Metallurgica*, vol. 21, pp. 571–574.

Murakami, H. (1986): Laminated composite plate theory with improved in-plane responses. *J. Appl. Mech.,* vol. 53, pp. 661–666.

Noor, A.K.; Burton, W.S. (1990a): Assessment of computational models for multilayered anisotropic plates. *Compos. Struct.*, vol. 14, pp. 233–265.

Noor, A.K.; Burton, W.S. (1990b): Assessment of computational models for multilayered composite shells. *Appl. Mech. Rev.*, vol. 43, pp. 67–97.

Noor, A.K.; Burton W.S. (1990c): Three-dimensional solutions for antisymmetrically laminated anisotropic plates. *J. Appl. Mech.*, vol. 57, pp. 182–188.

Noor, A.K.; Burton, W.S. (1992): Computational models for high-temperature multilayered composite plates and shells. *Appl. Mech. Rev.*, vol. 45, pp. 419–446.

Pagano, N.J. (1969): Exact solutions for composite laminates in cylindrical bending. *J. Compos. Mater.*, vol. 3, pp. 398–411.

Pagano, N.J. (1970): Exact solutions for rectangular bidirectional composite and sandwich plates. *J. Compos. Mater.*, vol. 4, pp. 20–34.

Pan, E. (2003): Exact solution for functionally graded anisotropic elastic composite laminates. *J. Compos. Mater.*, vol. 37, pp. 1903–1920.

Pan, E.; Han, F. (2005): Exact solution for functionally graded and layered magneto-electro-elastic plates. *Int. J. Eng. Sci.*, vol. 43, pp. 321–339.

Pan, E.; Heyliger, P.R. (2002): Free vibration of simply supported and multilayered magneto-electro-elastic plates. *J. Sound Vib.*, vol. 252, pp. 429–442.

Ramirez, F.; Heyliger, P.R.; Pan, E. (2006a): Static analysis of functionally graded elastic anisotropic plates using a discrete layer approach. *Compos. Part B: Eng.*, vol. 37, pp. 10–20.

Ramirez, F.; Heyliger, P.R.; Pan, E. (2006b) Discrete layer solution to free vibrations of functionally graded magneto-electro-elastic plates. *Mech. Adv. Mater. Struct.*, vol. 13, pp. 249–266.

Reddy, J.N.; Phan, N.D. (1985): Stability and vibration of isotropic, orthotropic

and laminated plates according to a higher-order shear deformation theory. *J. Sound Vib.*, vol. 98, pp. 157–170.

Reissner, E. (1984): On a certain mixed variational theory and a proposed applications. *Int. J. Numer. Methods Eng.*, vol. 20, pp. 1366–1368.

Reissner, E. (1986): On a mixed variational theorem and on a shear deformable plate theory. *Int. J. Numer. Methods Eng.*, vol. 23, pp. 193–198.

Saravanos, D. A.; Heyliger, P. R. (1999): Mechanics and computational models for laminated piezoelectric beams, plates, and shells. *Appl. Mech. Rev.*, vol. 52, pp. 305–319.

Saravanos, D.A.; Heyliger, P.R.; Hopkins, D.A. (1997): Layerwise mechanics and finite element for the dynamic analysis of piezoelectric composite plates. *Int. J. Solids Struct.*, vol. 34, pp. 359–378.

Savoia, M.; Reddy J.N. (1995): Three-dimensional thermal analysis of laminated composite plates. *Int. J. Solids Struct.*, vol. 32, pp. 593–608.

Sciuva, M.D. (1986): Bending, vibration and buckling of simply supported thick multilayered orthotropic plates: An evaluation of a new displacement model. *J. Sound Vib.*, vol. 105, pp. 425–442.

Soldatos, K.P. (1994): Review of three-dimensional dynamic analyses of circular cylinders and cylindrical shells. *Appl. Mech. Rev.*, vol. 47, pp. 501–516.

Srinivas, S.; Rao, A.K. (1970): Bending, vibration and buckling of simply supported thick orthotropic rectangular plates and laminates. *Int. J. Solids Struct.*, vol. 6, pp. 1463–1481.

Tang, Y.Y.; Noor, A.K.; Xu, K. (1996): Assessment of computational models for thermoelectroelastic multilayered plates. *Comput. Struct.*, vol. 61, pp. 915–933.

Toledano, A.; Murakami, H. (1987): A high-order laminated plate theory with improved in-plane responses. *Int. J. Solids Struct.*, vol. 23, pp. 111–131.

Vel, S.S.; Batra R.C. (2001): Exact solution for the cylindrical bending of laminated plates with embedded piezoelectric shear actuators. *Smart Mater. Struct.*, vol. 10, pp. 240–251.

Vel, S.S.; Batra, R.C. (2002): Exact solution for thermoelastic deformations of functionally graded thick rectangular plates. *AIAA J.*, vol. 40, pp. 1421–1433.

Vel, S.S.; Batra, R.C. (2003): Three-dimensional analysis of transient thermal stresses in functionally graded plates. *Int. J. Solids Struct.*, vol. 40, pp. 7181–7196.

Vel, S.S.; Batra, R.C. (2004): Three-dimensional exact solution for the vibration of functionally graded rectangular plates. *J. Sound Vib.*, vol. 272, pp. 703–730.

Whitney, J.M.; Pagano, N.J. (1970): Shear deformation in heterogeneous anisotropic plates. *J. Appl. Mech.*, vol. 37, pp. 1031–1036.

Wu, C.P.; Chen, W.Y. (1994): Vibration and stability of laminated plates based on a local high order plate theory. *J. Sound Vib.*, vol. 177, pp. 503–520.

Wu, C.P.; Chiu, K.H.; Wang, Y.M. (2008): A review on the three-dimensional analytical approaches of multilayered and functionally graded piezoelectric plates and shells. *CMC: Comput. Mater. Continua*, vol. 8, pp. 93–132.

Wu, C.P.; Chiu, K.H.; Wang, Y.M. (2011): RMVT-based meshless collocation and element-free Galerkin methods for the quasi-3D analysis of multilayered composite and FGM plates. *Compos. Struct.* vol. 93, pp. 923–943.

Wu, C.P.; Kuo, H.C. (1992): Interlaminar stresses analysis for laminated composite plates based on a local high order lamination theory. *Compos. Struct.*, vol. 20, pp. 237–247.

Wu, C.P.; Kuo, H.C. (1993): An interlaminar stress mixed finite element method for the analysis of thick laminated composite plates. *Compos. Struct.*, vol. 24, pp. 29–42.

Wu, C.P.; Li, H.Y. (2010a): An RMVT-based third-order shear deformation theory of multilayered functionally graded material plates. *Compos. Struct.*, vol. 92, pp. 2591–2605.

Wu, C.P.; Li, H.Y. (2010b): The RMVT- and PVD-based finite layer methods for the three-dimensional analysis of multilayered composite and FGM plates. *Compos. Struct.*, vol. 92, pp. 2476–2496.

Wu, C.P.; Lü, Y.C. (2009): A modified Pagano method for the 3D dynamic responses of functionally graded magneto-electro-elastic plates. *Compos. Struct.*, vol. 90, pp. 363–372.

Wu, C.P.; Tarn, J.Q.; Chi, S.M. (1996): An asymptotic theory for dynamic response of doubly curved laminated shells. *Int. J. Solids Struct.*, vol. 33, pp. 3813–3841.

Wu, C.P.; Tarn, J.Q.; Tang, S.C. (1998): A refined asymptotic theory for dynamic analysis of doubly curved laminated shells. *Int. J. Solids Struct.*, vol. 35, pp. 1953–1979.

Wu, C.P.; Tsai, Y.H. (2009): Cylindrical bending vibration of functionally graded piezoelectric shells using the method of perturbation. *J. Eng. Math.*, vol. 63, pp. 95–119.

Wu, C.P.; Tsai, Y.H. (2010): Dynamic responses of functionally graded magneto-electro-elastic shells with closed-circuit surface conditions using the method of multiple scales. *Eur. J. Mech. A/Solids*, vol. 29, pp. 166–181.

Wu, C.P.; Wu, C.H. (2000): Asymptotic differential quadrature solutions for the free vibration of laminated conical shells. *Comput. Mech*., vol. 25, pp. 346–357.

Zenkour, A.M. (2006): generalized shear deformation theory for bending analysis of functionally graded plates. *Appl. Math. Model*, vol. 30, pp. 67–84.

Zenkour, A.M. (2007): Three-dimensional elasticity solution for uniformly loaded cross-ply laminates and sandwich plates. *J. Sandw. Struct. Mater.*, vol. 9, pp. 213–238.